

Detailed analysis of the decay spectrum of a super-heavy X particle

Cyrille Barbot and Manuel Drees

Physik Dept., TU München, James Franck Str., D-85748 Garching, Germany

Abstract

Decays of superheavy X particles with mass $M_X \sim 10^{12} - 10^{16}$ GeV have been proposed as origin of the observed ultra high energy cosmic rays (UHECR). We describe in detail the physics involved in the different steps of the decay of such a particle. In particular, we give for the first time the complete set of splitting functions needed to model a parton shower in the minimal supersymmetric extension of the Standard Model (MSSM). We present our results in the form of fragmentation functions of any (s)particle of the MSSM into any final stable particle (proton, photon, electron, three types of neutrino, lightest superparticle LSP) at a virtuality $Q = M_X$, over a scaled energy range $x \equiv 2E/M_X \in [10^{-13}, 1]$. Extending the coverage to such small fractional energies is necessary since the energy region around 10^{18} eV and below could be of considerable interest in testing this kind of model for generating UHECR. We explicitly demonstrate that our treatment conserves energy, and discuss the dependence of the final result on SUSY parameters. We also show that our results are essentially independent of the necessary extrapolation of the input fragmentation functions, which are known only for $x \geq 0.1$, towards small x . Finally, we added a new treatment of the color coherence effects at very small x , using the analytic “MLLA” solution. Our computer code will soon be made available.

1 Introduction

In the last few decades ultrahigh energy cosmic rays (UHECR), with energy above the so-called GZK cut-off [1], have been observed [2]. The classical “bottom-up” explanation for the acceleration of CR particles exploits the electromagnetic fields that are likely to be present in objects like gamma ray bursters [3], “hot spots” of radio-galaxies [4] or near super-massive black holes in dormant quasars [5]. However, it is difficult to find objects capable of accelerating protons to energies above 10^{20} eV, partly because the product of field strength and spatial extension of the field does not seem to be sufficiently large, and partly because the accelerated particles can lose a fair fraction of their energy in synchrotron radiation. As an attractive alternative, “top-down” models have been proposed. Here one postulates the existence of “new physics” at a very high energy scale, i.e. the existence of super-heavy particles of masses greater than 10^{12} GeV, which could decay and hence produce the observed UHECR; this idea has been reviewed e.g. in [6, 7]. The existence of such a very high energy scale strongly suggests the existence of superparticles with masses not much above 1 TeV in order to guarantee the perturbative stability of the hierarchy between M_X and the weak scale. We therefore usually allow superparticles as well as ordinary particles to be produced in X decays, as described by the minimal supersymmetric extension of the Standard Model (MSSM).

Among the top-down scenarios, we have to distinguish between (at least) two classes of X particles: GUT particles (gauge or Higgs bosons of masses close to the GUT scale $\sim 10^{16}$ GeV) could be trapped in topological defects (cosmic strings or monopoles) formed during a phase transition in the early Universe, and might be released when these defects annihilate or collapse [8, 9]. Another possibility is to consider metastable X particles [10] that are distributed freely in the Universe; they might have been created at the end of inflation [11]. If their lifetime τ_X exceeds the age of the Universe by about a factor $10^{10} \cdot (10^{12} \text{ GeV})/M_X$, the X density required to explain the observed flux of UHECR events also makes X a good cold Dark Matter candidate [12, 13]. Depending on the model we are considering, X decay modes can be very different. For example, GUT gauge bosons will undergo two-body decays into all light (MS)SM particles with comparable branching ratios. On the other hand, if X decays only proceed through higher dimensional operators, X will usually undergo many-body decays. In another recently proposed “brane world” scenario [14], Γ_X is exponentially suppressed by the relatively large distance between two branes, and X decays predominantly into light Higgs bosons and their superpartners. In any case, it is reasonable to assume that X will decay into some light particles contained in the spectrum of the MSSM. These primary decay products initiate parton cascades, the development of which can be predicted from the “known” interactions contained in the MSSM.

Here we describe in detail the calculation of the spectrum of stable particles (protons, electrons, photons, three kinds of neutrinos, and lightest superparticles LSP) produced in X decays; a brief summary of these results has appeared in [15]. The first calculations of this kind [8] used simple scaling fragmentation functions to describe the transition from partons to hadrons. Later analyses [13, 16] used Monte Carlo programs to describe the cascade. However, since we can only expect to see a single particle from any given cascade, we only need to know

the one-particle inclusive decay spectrum of X . This is encoded in fragmentation functions; the evolution of the cascade corresponds to the scale dependence of these FFs, which is described by generalized DGLAP equations [17]. In contrast to earlier analyses using this technique, which only include (SUSY) QCD [18, 19, 20, 21], or at best a partial treatment of electroweak interactions [22, 23], we consider all gauge interactions as well as third generation Yukawa interactions; note that at energies above 10^{20} eV, due to the running of the coupling constants, all gauge interactions are of comparable strength. We will show that the inclusion of electroweak gauge interactions in the shower gives rise to a significant flux of very energetic photons and leptons, beyond the highest proton energies. Moreover, we carefully model decays of all unstable particles. As a result, we are for the first time able to fully account for the energy released in X decay. We cover all possible primary X decay modes, i.e. our results should be applicable to all models where physics at energies below M_X is described by the MSSM.

Before going into technical details, we briefly outline the physics involved in the decay of an ultra-heavy X particle; it is summarized in fig. 1. By assumption its primary decay is into 2 or more particles of the MSSM. These primary decay products will generally not be on-shell; instead, they have very large (time-like) virtualities, of order M_X . Each particle produced in the primary decay will therefore initiate a parton shower. The basic mechanism driving the shower development is the splitting of a virtual particle into two other particles with (much) smaller virtualities; the dynamics of this process is described by a set of splitting functions (SFs). As long as the virtuality is larger than the typical sparticle mass scale M_{SUSY} , all MSSM particles participate in this shower. At virtuality $M_{\text{SUSY}} \sim 1$ TeV the breaking of both supersymmetry and of $SU(2) \times U(1)_Y$ gauge invariance becomes important. All the massive superparticles that have been produced at this stage can now be considered to be on-shell, and will decay into Standard Model (SM) particles and the only (possibly) stable sparticle, the LSP. The same is true for the heavy SM particles, i.e. the top quarks and the massive bosons. However, the lighter quarks and gluons will continue a perturbative parton shower until they have reached either their on-shell mass scale or the typical scale of hadronization $Q_{\text{had}} \sim 1$ GeV. At this stage, strong interactions become non-perturbative, forcing partons to hadronize into colorless mesons or baryons. Finally, the unstable hadrons and leptons will also decay, and only the stable particles will remain. The spectra of these particles constitute the result of our calculation, which gives the UHECR spectrum at the location of X decay. Of course, the spectrum on Earth might be modified considerably due to propagation through the (extra)galactic medium [6]; we will not address this issue here.

Technically the shower development is described through fragmentation functions (FFs). The dependence of these functions on the virtuality is governed by the DGLAP evolution equations [17] extended to include the complete spectrum of the MSSM. All splitting functions needed in this calculation are collected in Appendix A. We numerically solved the evolution equations for the FFs of any particle of the MSSM into any other. At scale M_{SUSY} we applied unitary transformations to the FFs of the unbroken fields (“current eigenstates”) in order to obtain those of the physical particles (“mass eigenstates”); details are given in Appendix B. We then model the decays of all particles and superparticles with mass $\sim M_{\text{SUSY}}$, using the public

per mille.

The remainder of this article is organized as follows. In sec. 2 we describe the technical aspects of the calculation. The derivation and solution of the evolution equations is outlined. We also check that our final results are not sensitive to the necessary extrapolation of the input FFs. Numerical results are presented in sec. 3. We give the energy fractions carried by the seven stable particles for any primary X decay product, and study the dependence of our results on the SUSY parameters. We finally describe our implementation of color coherence effects at small x using the modified leading log approximation (MLLA). Sec. 4 is devoted to a brief summary and conclusions. Technical details are delegated to a series of Appendices, giving the complete list of splitting functions, the unitary transformations from the interaction states to the physical states, our treatment of 2- and 3-body decays, parameterizations of the input FFs, and finally a complete set of FFs obtained with our program for a given set of SUSY parameters (corresponding to a gaugino-like LSP with a low value of $\tan\beta \sim 3.6$ and $M_{\text{SUSY}} \sim 500$ GeV).

2 Technical aspects of the calculation

In this section we describe how to calculate the spectra of stable particles produced in X decays: protons, electrons, photons, the three types of neutrinos and LSPs, and their antiparticles. Note that at most one out of the many particles produced in a typical X decay will be observed on Earth. This means that we cannot possibly measure any correlation between different particles in the shower; the energy spectra of the final stable particles are indeed the only measurable quantities. These spectra are given by the differential decay rates $d\Gamma_X/dE_P$, where P labels the stable particle we are interested in. This is a well-known problem in QCD, where parton showers were first studied. The resulting spectrum can be written in the form [26]

$$\frac{d\Gamma_X}{dx_P} = \sum_I \frac{d\Gamma(X \rightarrow I)}{dx_I} \otimes D_I^P\left(\frac{x_P}{x_I}, M_X^2\right), \quad (1)$$

where I labels the MSSM particles into which X can decay, and we have introduced the scaled energy variable $x = 2E/M_X$. $d\Gamma(X \rightarrow I)/dx_I$ depends on the phase space in a particular decay mode; for a two-body decay, $d\Gamma(X \rightarrow I)/dx_I \propto \delta(1 - x_I)$. The convolution is defined as

$$f(z) \otimes g(x/z) = \int_x^1 f(z)g\left(\frac{x}{z}\right) \frac{dz}{z}. \quad (2)$$

All the nontrivial physics is now contained in the fragmentation functions (FFs) $D_I^P(z, Q^2)$. They encode the probability for a particle P to originate from the shower initiated by another particle I , where the latter has been produced with initial virtuality Q . This implies the “boundary conditions”

$$D_I^J(z, m_J^2) = \delta_I^J \cdot \delta(1 - z), \quad (3)$$

which simply say that an on-shell particle cannot participate in the shower any more. As already explained in the Introduction, for $Q > M_{\text{SUSY}}$ all MSSM particles J are active in the shower, and thus have to be included in the list of “fragmentation products”.

The evolution of the FFs with increasing virtuality is described by the well-known DGLAP equations [17]. In the next two subsections we discuss these evolution equations, and their solution, in more detail. We first only include strong (SUSY–QCD) interactions. However, at energies above 10^{20} eV all gauge interactions are of comparable strength. The same is true for interactions due to the Yukawa coupling of the top quark, and possibly also for those of the bottom quark and tau lepton. In a second step we therefore extend the evolution equations to include these six different interactions. We then describe the decays of heavy (s)particles, which happen at virtuality $Q = M_{\text{SUSY}} \sim 1$ TeV. At $Q < M_{\text{SUSY}}$ only QCD interactions need to be included, greatly simplifying the treatment of the evolution equations in this domain. Finally, we describe the nonperturbative hadronization, and the weak decays of unstable hadrons and leptons.

2.1 Evolution equations in QCD and SUSY–QCD

For convenience, we review here the DGLAP evolution equations in ordinary QCD. As already noted, the FF $D_p^P(x, Q^2)$ of a parton (quark or gluon) p into a particle (parton or hadron) P describes the probability of fragmentation of p into P carrying energy $E_P = xE_p$ at a virtuality scale Q . If P is itself a parton, the FF has to obey the boundary condition (3). However, if P is a hadron, the x –dependence of the FF cannot be computed perturbatively; it is usually derived from fits to experimental data. Perturbation theory does predict the dependence of the FFs on the virtuality Q : it is described by a set of coupled integro–differential equations. In leading order (LO), these QCD DGLAP evolution equations can be written as [26] :

$$\begin{aligned} \frac{dD_{q_i}^P(x, Q^2)}{d \log(Q^2)} &= \frac{\alpha_S(Q^2)}{2\pi} \left\{ P_{gq}(z) \otimes D_g^P\left(\frac{x}{z}, Q^2\right) + P_{qq}(z) \otimes D_{q_i}^P\left(\frac{x}{z}, Q^2\right) \right\}, \\ \frac{dD_g^P(x, Q^2)}{d \log(Q^2)} &= \frac{\alpha_S(Q^2)}{2\pi} \left\{ P_{gg}(z) \otimes D_g^P\left(\frac{x}{z}, Q^2\right) + \sum_{i=1}^{2F} P_{qg}(x) \otimes D_{q_i}^P\left(\frac{x}{z}, Q^2\right) \right\}, \end{aligned} \quad (4)$$

where α_S is the running QCD coupling constant, F is the number of active flavors (i.e. the number of Dirac quarks whose mass is lower than Q), and i labels the quarks and antiquarks.[†] The convolution has been defined in eq.(2). The physical content of these equations can be understood as follows. A virtual quark q_i can reduce its virtuality by emitting a gluon; the final state then contains a quark and a gluon. Either of these partons (with reduced virtuality) can fragment into the desired particle P ; this explains the occurrence of two terms in the first eq.(4). Analogously, a gluon can either split into two gluons, or into a quark–antiquark pair, giving rise to the two terms in the second eq.(4).

These partonic branching processes are described by the splitting functions (SFs) $P_{p_2 p_1}(x)$, for parton p_1 splitting into parton p_2 , where $x = E_{p_2}/E_{p_1}$. As already noted, in pure QCD there

[†]Note that the DGLAP equations given here are the *time-like* ones, which describe the evolution of fragmentation functions. In leading order they differ from the *space-like* DGLAP equation (describing the evolution of distribution functions of partons inside hadrons) only through a transposition of the matrix of the splitting functions.

are only three such processes: gluon emission off a quark or gluon, and gluon splitting into a $q\bar{q}$ pair. The first of these processes gives rise to both SFs appearing in the first eq.(4); momentum conservation then implies $P_{qq}(x) = P_{gq}(1-x)$, for $x \neq 1$. Similarly, $P_{gg}(x) = P_{gq}(1-x)$ and $P_{qg}(x) = P_{gg}(1-x)$ follows from the symmetry of the final states resulting from the splitting of a gluon. Special care must be taken as $x \rightarrow 1$. Here one encounters infrared singularities, which cancel against virtual quantum corrections. The physical result of this cancellation is that the energy of the fragmenting parton p is conserved, which requires

$$\sum_P \int_0^1 x D_p^P(x, Q^2) = 1 \quad \forall p, Q^2. \quad (5)$$

This can be ensured, if

$$\int_0^1 dx x \sum_{p'} P_{p'p}(x) = 0 \quad \forall p. \quad (6)$$

Note that these integrals must give zero (rather than one), since eqs.(4) only describe the *change* of the FFs. The explicit form of the QCD SFs is [17]:

$$\begin{aligned} P_{qq}(x) &= \frac{4}{3} \left(\frac{1+x^2}{1-x} \right)_+, \\ P_{gq}(x) &= \frac{4}{3} \frac{1+(1-x)^2}{x}, \\ P_{qg}(x) &= \frac{1}{2} \left[(1-x)^2 + x^2 \right], \\ P_{gg}(x) &= 6 \left[\frac{1-x}{x} + x(1-x) + \frac{x}{(1-x)_+} + \delta(1-x) \left(\frac{11}{12} - \frac{F}{18} \right) \right]. \end{aligned} \quad (7)$$

The “+” distribution, which results from the cancellation of $x \rightarrow 1$ divergences as outlined above, is defined as:

$$\int_0^1 f(x)g(x)_+ dx = \int_0^1 [f(x) - f(1)]g(x) dx, \quad (8)$$

while $g(x)_+ = g(x)$ for $x \neq 1$. Finally, the scale dependence of $\alpha_S(Q^2)$ is described by the following solution of the relevant renormalization group equation (RGE):

$$\alpha_S(Q^2) = \frac{2\pi B}{\log \frac{Q^2}{\Lambda^2}}, \quad (9)$$

where $\Lambda \sim 200$ MeV is the QCD scale parameter, and $B = 6/(33 - 2F)$.

Note that eqs.(4) list different FFs for all (anti)quark flavors q_i . At first sight it thus seems that one has to deal with a system of $2F + 1$ coupled equations. In practice the situation can be simplified considerably by using the linearity of the evolution equations. This implies

$$D_p^P(x, Q^2) = \sum_{p'} \tilde{D}_p^{p'}(z, Q^2, Q_0^2) \otimes D_{p'}^P\left(\frac{x}{z}, Q_0^2\right), \quad (10)$$

where the generalized FFs $\tilde{D}_p^{p'}$ again obey the evolution equations (4). Moreover, they satisfy the boundary conditions $D_p^{p'}(x, Q_0^2, Q_0^2) = \delta(1-x)\delta_p^{p'}$ at some convenient value of $Q_0 < Q$. The \tilde{D} thus describe the purely perturbative evolution of the shower between virtualities Q and Q_0 . This ansatz simplifies our task, since all quark flavors have exactly the same strong interactions, i.e. we can use the *same* $\tilde{D}_{q_i}^{p'}$ for all quarks q_i with $m_{q_i} < Q_0$. Moreover, we only have to distinguish three different cases for $p' : q_i, q_j$ with $j \neq i$, and g . All flavor dependence is then described by the $D_{p'}^P(x, Q_0^2)$; for sufficiently small Q_0 , these can be taken directly from fits to experimental data. If we make the additional simplifying assumption that all quarks and antiquarks are produced with equal probability in primary X decays, we effectively only have to introduce two generalized FFs \tilde{D} for a given particle P , one for the fragmentation of gluons and one for the fragmentation of any quark. In other words, in pure QCD we only need to solve a system of two coupled equations.

The introduction of squarks \tilde{q}_i and gluinos \tilde{g} , i.e. the extension to SUSY–QCD, requires the introduction of FFs $D_{\tilde{q}_i}^P, D_{\tilde{g}}^P$. This gives rise to new SFs, describing the emission of a gluon by a squark or gluino, as well as splittings of the type $q_i \rightarrow \tilde{q}_i \tilde{g}$, $\tilde{q}_i \rightarrow q_i \tilde{g}$ and $\tilde{g} \rightarrow \tilde{q}_i \tilde{q}_i$. We thus see that any of the four types of partons ($q_i, \tilde{q}_i, g, \tilde{g}$) can split into any (other) parton. The complete set of evolution equations thus contains 16 SFs [27], which we collect in Appendix A. The presence of new particles with $SU(3)$ interactions also modifies the running of α_S . One can still use eq.(9), but now $B_{SUSY} = 2/(9 - F)$.

2.2 Evolution equations in the MSSM

We now extend our discussion of the evolution equations to the full MSSM. We already saw in the Introduction that superparticles can only be active in the shower evolution at virtualities $Q > M_{SUSY} \sim 1$ TeV. This means that the supersymmetric part of the shower evolution can be described in terms of generalized FFs \tilde{D}_I^J satisfying the boundary condition

$$\tilde{D}_I^J(x, M_{SUSY}^2, M_{SUSY}^2) = \delta_I^J \delta(1-x), \quad (11)$$

where I and J label any (s)particle contained in the MSSM. Note that eq.(11) differs from eq.(3) since the former is valid for *all* particles in the MSSM, including light partons. According to the discussion following eq.(10) we only have to consider those particles to be distinct that have different interactions. We include all gauge interactions in this part of the shower evolution, as well as the Yukawa interactions of third generation (s)fermions and Higgs bosons, but we ignore first and second generation Yukawa couplings, as well as all interactions between different generations. This immediately implies that we do not need to distinguish between first and second generation particles. Moreover, we ignore CP violation, which means that we need not distinguish between particles and antiparticles. Finally, the electroweak $SU(2)$ symmetry can be taken to be exact at virtuality $Q > M_{SUSY}$, i.e. we need not distinguish between members of the same $SU(2)$ multiplet. This is analogous to ordinary QCD, where one does not need to introduce different FFs for quarks with different colors. Our assumption implies that X is an $SU(2)$ singlet. Had we allowed [23] X to transform nontrivially under $SU(2)$, the $SU(2)$

splitting functions would have to be modified [28].[‡]

Altogether we therefore need to treat 30 distinct particles: six quarks $q_L, u_R, d_R, t_L, t_R, b_R$, four leptons l_L, e_R, τ_L, τ_R , three gauge bosons B, W, g , two Higgs bosons H_1, H_2 , and all their superpartners; H_1 couples to down-type quarks and leptons, while H_2 couples to up-type quarks. Note that a “particle” often really describes the contribution of several particles which are indistinguishable by our criteria. For example, the “quark” u_R stands for all charge- $2/3$ right-handed quarks and antiquarks of the two first generations, i.e. u_R, c_R and their antiparticles \bar{u}_R, \bar{c}_R . This can be expressed formally as $D_{u_R}^P = (D_{u_R}^P + D_{c_R}^P + D_{\bar{u}_R}^P + D_{\bar{c}_R}^P)/4$, where in our approximation the four terms in the sum are all identical to each other after the final state P has been summed over particle and antiparticle.[§] Similarly, q_L stands as initial particle for an average over the two $SU(2)$ quark doublets of the two first generations (u_L, d_L) and (c_L, s_L), and their antiparticles. Note that all group indices of the particle in question are summed over. In the usual case of QCD this only includes summation over color indices, but in our case it includes summation over $SU(2)$ indices, since $SU(2)$ is (effectively) conserved at energies above M_{SUSY} .

Let us first discuss the scale dependence of the six coupling constants that can affect the shower evolution significantly at scales $Q > M_{\text{SUSY}}$. These are the three gauge couplings g_Y, g_2 and g_S , which are related to the corresponding “fine structure constants” through $\alpha_i \equiv g_i^2/(4\pi)$, $i \in \{Y, 2, S\}$. Moreover, the third generation Yukawa couplings are proportional to the masses of third generation quarks or leptons:

$$\begin{aligned} y_t &= \frac{g m_t}{\sqrt{2} m_W \sin \beta}, \\ y_b &= \frac{g m_b}{\sqrt{2} m_W \cos \beta}, \\ y_\tau &= \frac{g m_\tau}{\sqrt{2} m_W \cos \beta}, \end{aligned} \tag{12}$$

where $\tan \beta \equiv \langle H_2^0 \rangle / \langle H_1^0 \rangle$. The couplings y_b and y_τ are only significant if $\tan \beta \gg 1$. Note that in many models, values $\tan \beta \simeq m_t(m_t)/m_b(m_t) \simeq 60$ are possible, in which case y_b and

[‡]A minor caveat might be in order here. We assume the electroweak part of the evolution of the FFs to be described by the equations for an unbroken $SU(2) \times U(1)_Y$ theory. It seems physically reasonable that this should be a good approximation as long as both the energy and the virtuality of the gauge bosons is large compared to their masses, which is the case in our calculation. Indeed, existing loop calculations [29] confirm that the leading logarithmic corrections, which we treat here, are the same in the broken and unbroken theory, as long as all scales are large compared to M_W . However, these calculations all deal with the electroweak equivalent of structure functions, rather than fragmentation functions. Strictly speaking our assumption, although reasonable, has therefore not yet been backed up by an explicit calculation that includes massive gauge bosons.

[§]A consistent interpretation of, e.g., u_R as a “particle” requires that u_R stands for the *average* of u_R, c_R etc. when u_R appears as *lower* index of a generalized FF, as described in the text. However, u_R stands for the *sum* of u_R, c_R etc. when u_R is an *upper* index of a \tilde{D} . With this definition, we have $\tilde{D}_{u_R}^{u_R}(x, M_{\text{SUSY}}^2) = \delta(1-x)$. This interpretation also fixes certain multiplicity factors in the DGLAP equations, as detailed in Appendix A. This treatment is only possible if X has equal branching ratio into u_R, c_R etc. However, we expect the differences between decays into first or second generation quarks to be very small even in models where these branching ratios are not the same.

y_τ are comparable in magnitude to g_S and g_2 , respectively. The LO RGEs for these six MSSM couplings are [30]:

$$\begin{aligned}
\frac{dg_Y}{dt} &= 11 \frac{g_Y^3}{16\pi^2}, \\
\frac{dg_2}{dt} &= \frac{g_2^3}{16\pi^2}, \\
\frac{dg_S}{dt} &= -3 \frac{g_S^3}{16\pi^2}, \\
\frac{dy_t}{dt} &= \frac{y_t}{16\pi^2} \left(6y_t^2 + y_b^2 - \frac{13}{9}g_Y^2 - 3g_2^2 - \frac{16}{3}g_S^2 \right), \\
\frac{dy_b}{dt} &= \frac{y_b}{16\pi^2} \left(6y_b^2 + y_t^2 + y_\tau^2 - \frac{7}{9}g_Y^2 - 3g_2^2 - \frac{16}{3}g_S^2 \right), \\
\frac{dy_\tau}{dt} &= \frac{y_\tau}{16\pi^2} \left(3y_b^2 + 4y_\tau^2 - 3g_Y^2 - 3g_2^2 \right),
\end{aligned} \tag{13}$$

where $t = \log \frac{Q}{Q_0}$ parameterizes the logarithm of the virtuality, and Q_0 is an arbitrary scale where the numerical values of these couplings constants are “known” (in case of the Yukawa couplings, up to the dependence on $\tan \beta$). As well known [31], given their values measured at $Q_0 \simeq 100$ GeV eqs.(13) predict the three gauge couplings to unify at scale $M_{\text{GUT}} \simeq 2 \cdot 10^{16}$ GeV, i.e. $g_3^2(M_{\text{GUT}}) = g_2^2(M_{\text{GUT}}) = 5g_Y^2(M_{\text{GUT}})/3 \simeq 0.52$, where the Clebsch–Gordon factor of 5/3 is predicted by most simple unified groups, e.g. $SU(5)$ or $SO(10)$. We solved these equations by the Runge–Kutta method; of course, the RGEs for the gauge couplings can trivially be solved analytically, but the additional numerical effort required by including eqs.(13) in the set of coupled differential equations that need to be solved numerically is negligible.

The main numerical effort lies in the solution of the system of 30 coupled DGLAP equations, which are of the form:

$$\frac{d\tilde{D}_I^J}{d \log(Q^2)}(x, Q^2, M_{\text{SUSY}}^2) = \sum_K \frac{\alpha_{KI}(Q^2)}{2\pi} P_{KI}(z) \otimes \tilde{D}_K^J\left(\frac{x}{z}, Q^2, M_{\text{SUSY}}^2\right), \tag{14}$$

where I, J, K run over all the 30 particles, and $\alpha_{KI}(Q^2) = g_{KI}^2/4\pi$ is the (running) coupling constant associated with the corresponding vertex; note that at this stage we are using interaction (or current) eigenstates to describe the spectrum. Generically denoting particles with spin 1, 1/2 and 0 as V , F and S (for vector, fermion and scalar), we have to consider* branching processes of the kind $V \rightarrow VV$, $V \rightarrow FF$, $V \rightarrow SS$, $F \rightarrow FV$, $F \rightarrow FS$, $S \rightarrow SV$ and $S \rightarrow FF$. All these branching processes already occur in SUSY–QCD. The splitting functions can thus essentially be read off from the results of ref.[27], after correcting for different group [color and/or $SU(2)$] and multiplicity factors. The coefficients of the $\delta(1-x)$ terms in diagonal SFs can be fixed using the momentum conservation constraint in the form (6); note that these

*We do not need to consider $S \rightarrow SS$, since the corresponding dimensionful coupling is $\mathcal{O}(M_{\text{SUSY}}) \ll Q$ in this domain, i.e. these processes are much slower than the relevant time scale $1/Q$.

constraints have to be satisfied for each of the six interactions separately. The explicit form of the complete set of MSSM SFs $P_{KI}(x)$ is given in Appendix A.

We solved these equations numerically using the Runge–Kutta method. To that end the FFs were represented as cubic splines, using 50 points which were distributed equally on a logarithmic scale in x for $10^{-7} \leq x \leq 0.5$, and 50 additional points distributed equally in $\log(1-x)$ for $0.5 \leq x \leq 1 - 10^{-7}$. Starting from the boundary conditions[†] (11), we arrive at the 30×30 generalized fragmentation functions at virtuality $Q = M_X$. Here we assume that the evolution equations describe the perturbative cascade at these energies correctly. We will comment on the limitations of our treatment at the end of this Section.

2.3 Evolution of the cascade below $Q = 1$ TeV

Here we would like to describe the physics at scales at and below M_{SUSY} : the breaking of both supersymmetry and $SU(2) \otimes U(1)$ symmetry, the decay of unstable (s)particles with masses of order M_{SUSY} , the pure QCD shower evolution down to Q_{had} , the non-perturbative hadronization of quarks and gluons, and finally the weak decays of unstable leptons and hadrons. For simplicity we assume that all superparticles, the top quark as well as the W , Z and Higgs bosons all decouple from the shower and decay at the same scale $M_{\text{SUSY}} \simeq 1$ TeV. The fragmentation of b and c quarks is treated using the boundary condition (3) at their respective mass scales of 5 and 1.5 GeV, while the nonperturbative hadronization of all other partons takes place at $Q_{\text{had}} = 1$ GeV.

At $Q = M_{\text{SUSY}}$ we break both Supersymmetry and $SU(2) \otimes U(1)$. All (s)particles acquire their masses in this process, and in many cases mix to give the mass eigenstates. This means that we have to switch from a description of the particle spectrum in terms of current eigenstates to a description in terms of physical mass eigenstates. This is accomplished by unitary transformations of the type*

$$\tilde{D}_I^S = \sum_J |c_{SJ}|^2 \tilde{D}_I^J. \quad (15)$$

Unitarity requires $\sum_S |c_{SJ}|^2 = \sum_J |c_{SJ}|^2 = 1$, if the current state J has the same number of degrees of freedom as the physical state S . This is often not the case in the usual convention; then some care has to be taken in writing down the $|c_{SJ}|^2$, see Appendix B. We use the following physical particles: u, d, b, s, c, t quarks and e, μ, τ leptons now have both left- and right-handed components, i.e. they have twice as many degrees of freedom as the corresponding states with fixed chirality. The neutrinos remain unchanged, since we ignore the interactions of right-handed neutrinos. The gluons also remain unchanged, since $SU(3)$ remains exact below M_{SUSY} . The electroweak gauge sector of the SM is described by $W := W^+ + W^-$, Z and γ ; note that the massive gauge bosons absorb the Goldstone modes of the Higgs sector, and hence receive corresponding contributions in eq.(15). The Higgs sector consists of two charged

[†]Technically, these δ -functions are represented by narrow Gaussians centered at $x = 1$, normalized to give unity after integration over $x \leq 1$.

*Note that the squares of the coefficients c_{SJ} appear in eq.(15), since the FFs describe probabilities, which are related to the square of the wave functions of the particles in question.

Higgs bosons H^\pm (described by $H = H^+ + H^-$) and the three neutral ones H^0 , h^0 and A^0 ; the neutral Higgs bosons are described by real fields, which contain a single degree of freedom. In the SUSY part of the spectrum, the gluino \tilde{g} as well as the first and second generation sfermions $\tilde{u}_{L,R}$, $\tilde{d}_{L,R}$, $\tilde{s}_{L,R}$, $\tilde{c}_{L,R}$ and sneutrinos remain unchanged (but \tilde{u}_L and \tilde{d}_L , etc., are now distinguishable). The $SU(2)$ singlets and doublets of third generation charged sfermions mix to form mass eigenstates \tilde{t}_1 , \tilde{t}_2 , \tilde{b}_1 , \tilde{b}_2 , $\tilde{\tau}_1$, $\tilde{\tau}_2$. Similarly, the two Dirac charginos $\tilde{\chi}_1^\pm$ and $\tilde{\chi}_2^\pm$ are mixtures of charged higgsinos and winos, and the four Majorana neutralinos $\tilde{\chi}_1^0$, $\tilde{\chi}_2^0$, $\tilde{\chi}_3^0$, $\tilde{\chi}_4^0$, in order of increasing masses, are mixtures of neutral higgsinos, winos and binos.

The numerical values of many of the $c_{S,J}$ depend on the parameters describing the breaking of supersymmetry. We choose four different sets of parameters, which describe typical regions of the parameter space, in order to study the impact of the details of SUSY breaking on the final spectra. We take two fairly extreme values of $\tan(\beta) = 3.6$ and 48, and two sets of dimensionful parameters corresponding to higgsino-like and gaugino-like states $\tilde{\chi}_1^\pm$, $\tilde{\chi}_1^0$ and $\tilde{\chi}_2^0$. We used the software ISASUSY [24] to compute the mass spectrum and the mixing angles of the sparticles and Higgses for a given set of SUSY parameters.

Having computed the spectrum of physical (massive) particles, we have to treat the decay of all unstable particles with mass near M_{SUSY} . Since we assumed R -parity to be conserved, the lightest supersymmetric particle (LSP) is stable. In our four scenarios (as in most of parameter space) the LSP is the lightest neutralino $\tilde{\chi}_1^0$. The end products of these decays are thus light SM particles and LSPs. Note that decays of heavy sparticles often proceed via a cascade, where the LSP is produced only in the second, third or even fourth step, e.g. $\tilde{g} \rightarrow \tilde{u}\tilde{u}_L \rightarrow \bar{u}d\tilde{\chi}_1^+ \rightarrow \bar{u}de^+\nu_e\tilde{\chi}_1^0$. In order to model these decays we again use ISASUSY, which computes the branching ratios for all allowed tree-level 2- and 3-body decay modes of the unstable sparticles, of the top quark and of the Higgs bosons. Together with the known branching ratios of the W and Z bosons, this allows us to compute the spectra of the SM particles and the LSP after all decays, by convoluting the spectra of the decaying particles with the energy distributions calculated for 2- or 3-body decays. The total generalized FF of any MSSM current eigenstate I into a light or stable physical particle s (quark, gluon, lepton, photon or LSP) is then

$$\tilde{D}_I^s = \tilde{D}_I^{S=s} + \sum_{S \neq s} \tilde{D}_I^S \otimes \tilde{P}_{sS}, \quad (16)$$

where \tilde{P}_{sS} describes the spectrum of s in the decay $S \rightarrow s$. We compute these spectra from phase space, including all mass effects, but we didn't include the matrix elements. The spectra for each decay mode of the heavy particle S are normalized to give the correct branching ratio, as computed by ISAJET. As far as LSPs are concerned, eq.(16) already gives the final result, i.e. $D_I^{\text{LSP}} = \tilde{D}_I^{\text{LSP}}$. If s is a lepton or photon, eq.(16) describes the FF at all virtualities between M_{SUSY} and $m_b = 5$ GeV.

As we will see shortly, in some cases two-body decays can lead to sharp edges in the FFs at intermediate values of x . This can happen if the primary decay product is a massive particle with only weak interactions. In that case a substantial fraction of the initial δ -peak at $x = 1$ survives even after the evolution; convolution of this δ -peak with a two-body decay distribution leads to a flat x distribution of the decay products between some x_{min} and x_{max} . An accurate

description of these contributions to the FFs sometimes requires the introduction of additional points near x_{\min} and/or x_{\max} in the splines describing these FFs.

The perturbative evolution in the QCD sector does not stop at M_{SUSY} , but continues until virtuality $Q_0 = \max(m_q, Q_{\text{had}})$. This part can be treated by introducing generalized FFs $\tilde{D}_p^{p'}$ as in eq.(10), where $(p, p') \in \{u, d, s, c, b, g\}$ are light QCD partons. We use once more the DGLAP evolution equations, but this time for pure QCD, evolving these generalized FFs between Q_0 and M_{SUSY} . The generalized partonic FFs between Q_0 and M_X can then be computed through one more convolution:

$$\tilde{D}_I^p(x, M_X^2, Q_0^2) = \sum_{p'} \tilde{D}_I^{p'}(z, M_X^2, M_{\text{SUSY}}^2) \otimes \tilde{D}_{p'}^p\left(\frac{x}{z}, M_{\text{SUSY}}^2, Q_0^2\right). \quad (17)$$

The total partonic FFs at M_X can finally be computed through eq.(10) by using known “input FFs”. They describe the non-perturbative hadronization of quarks and gluons into mesons and baryons, which happens at $Q = Q_0$. These FFs $D_i^h(x, Q_0^2)$, where $i \in \{u, d, s, c, b, g\}$ and h represents a hadron, can be obtained directly from a fit to (e.g.) LEP data. We used the results of [25], where the FFs of a quark or gluon into protons, neutrons, pions and kaons (or more exactly the sum over particles and antiparticles) are parameterized in the form $Nx^\alpha(1-x)^\beta$.

The original form [25] of these functions is only valid down to $x = 0.1$. Kinematic and color coherence effects, which are not included in the usual DGLAP framework, become important [32]) at $x \lesssim \sqrt{(Q/Q_{\text{had}})} \sim 0.1$, where in the second step we have used the LEP energy scale $Q \sim 100$ GeV. For $Q \sim M_X \sim 10^{16}$ GeV these effects become large only for $x \lesssim 10^{-8}$; they can thus safely be ignored for many (but not all; see below) applications. In [15] we therefore chose a rather simple extrapolation of the functions given in [25] towards small x . Our default choice was a $Nx^{-\alpha'}$ parameterization; N and α' were computed by requiring the continuity of this parameterization with the FFs of [25] at some $x_0 \simeq 0.1$, energy conservation, and, as additional constraint, an identical power law behavior at small x (i.e. identical α') for all the FFs of a given quark into the different hadrons. This last assumption was motivated by the fact that we obtain such an identical power law at small x during the perturbative part of the cascade, and by the well accepted LPHD hypothesis (Local Parton-Hadron Duality) [33], which postulates a local proportionality in phase space between the spectra of partons and hadrons. We chose different x_0 for each initial parton in such a way that we obtain α' between 0 and 2; the upper bound on α' follows from energy conservation (the energy integral $\int_0^1 dx x D(x)$ has to be finite).

In order to check the consistency of this parameterization, we used another functional form with three free parameters: $D(x) = ax^{-\alpha'} + b \log x + c, a > 0$. This allowed us to freely choose α' , keeping the same assumptions about continuity etc. as above. This enabled us to compare two extreme values of α' , namely 0.5 and 1.4. The first is the smallest value compatible with $a > 0$, while the second approximates the small- x behavior of the perturbative QCD evolution between 1 GeV and 1 TeV; requiring $\alpha' < 1.4$ thus ensures that this perturbative evolution dominates the behavior of the FFs at small x . Note also that the perhaps most plausible value, $\alpha' \sim 1$ (which corresponds to a flat distribution of particles in rapidity when perturbative effects are ignored) is comfortably bracketed by these limiting values. In fig. 2 we

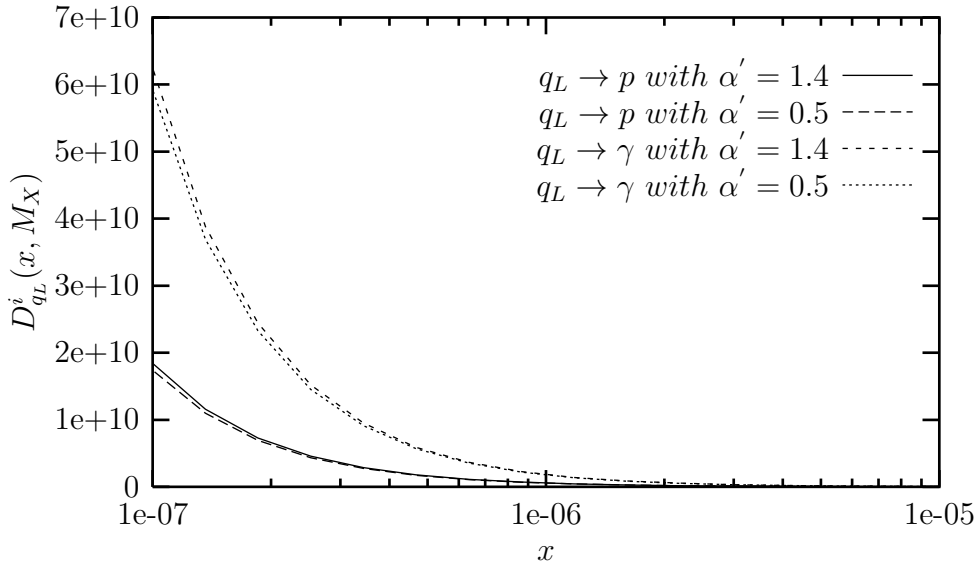


Figure 2: Effect of varying the low- x extrapolation of the input FFs on the final FFs $D_{q_L}^p$ and $D_{q_L}^\gamma$. See the text for further explanations.

plot the final result at small x for different FFs with these two extreme parameterizations, *after* convolution with the perturbative FFs. As can be seen, the effect of varying α' is very small once energy conservation is imposed. This indicates that our final results are not sensitive to the necessary small- x extrapolation of the input FFs.[†] The main uncertainty at moderately small x ($10^{-5} \lesssim x \lesssim 0.1$) will then come from perturbative higher order corrections, which might be quite significant in this range.

Unfortunately, we were not able to perform a complete NLO analysis, for the following reasons. Beyond leading order the SFs for space-like and time-like processes are no longer identical [34]. Already at next-to-leading order (NLO) the time-like SFs have a rather bad behavior at small x , with a negative leading term $-\frac{40}{9}\frac{1}{x}$ in P_{qq} . This term is tempered in the final spectra (which have to be positive) by the convolution occurring in the DGLAP equations, as well as by the convolution of the FFs with NLO “coefficient functions” which modify the basic relation (1) once higher order corrections are included. Note that the FFs, SFs and NLO coefficient functions are scheme dependent; worse, the coefficient functions are also process-dependent, i.e. they will depend on the spins of X and its primary decay products. NLO results are known for the classical processes occurring in pure (non-supersymmetric) QCD, but they are not available for most of the processes we are interested in. Moreover, in cases where they are known, these coefficient functions often contain the most important part of the NLO correction, rendering useless any attempt to give a partial result by only including NLO terms in the SFs. We conclude that it might be possible and interesting to carry out a full NLO

[†]However, the original FFs of ref.[25] should *not* be used on the whole range $[10^{-7}, 1]$, since they violate energy conservation badly, leading to over-production of particles at small x .

analysis in the pure QCD case, but this is not possible in the more interesting supersymmetric case using available results. Note that part of the perturbative NLO effects are absorbed in the input FFs, through their fit to experimental data. At very small x , NLO effects just give the leading “color coherence” corrections, which are resummed analytically in the MLLA formula, as will be discussed in Sec. 3.4.

Finally, having computed the spectra of long-lived hadrons and leptons, we still need to treat weak decays of unstable particles, in order to obtain the final spectra of protons, electrons, photons and the three types of neutrinos. This is again done using the formalism of eq.(16). We limit ourselves to 2- and 3-body decays, considering the 4-body decays of the τ to be cascades of 2-body decays. As before, we compute the decay functions P_{sH} for $H \rightarrow s$ decays from phase space only, and we ignore decays with branching ratio smaller than 1%. We then renormalize the branching ratios of the decays we do include, so that we maintain energy conservation. We also explicitly treated the leptonic part of the semi-leptonic decays of b - and c -flavored hadrons, which are evidently not included in the FFs of [25]. We used the Peterson parameterization for non-perturbative heavy quark fragmentation [35], and then treated the semi-leptonic decays in the spectator model (i.e. using the same spectra as for free quark decays, with $m_c = 1.5$ GeV and $m_b = 4.5$ GeV). Details of our treatment of decays are given in Appendix C.

3 Results and analysis

3.1 General features of the final fluxes

Some FFs computed with our code have already been presented in ref.[15]. In particular, we showed that including supersymmetric particles in the QCD shower evolution significantly softens the FFs of strongly interacting (s)particles. Usually FFs are multiplied with x^3 to allow a more direct comparison with the experimental UHECR spectra, which are multiplied with E^3 to make them (approximately) flat. In this normalization, including supersymmetry reduces the height of the peak of the FFs of initial quarks and gluons by approximately a factor of two. Including electroweak interactions reduces this peak by another 20% or so. More importantly, it leads to a very energetic component of the final FFs into leptons and especially photons, if the primary particle has electroweak interactions. This is due to the emission of very energetic electroweak gauge bosons early in the parton shower; some of them will decay or fragment (partly into leptonic final states), while others survive as photons after the unitary transformation (15). In this article we focus on a detailed description of X decays computed according to the “state of the art”, i.e. with all interactions included.

A fairly complete set of results of our code for a given set of SUSY parameters is given in Appendix E. Here we assumed similar masses for all sfermions, higgsinos, heavy Higgs bosons and gluinos, $m_{\tilde{f}} \simeq m_A \simeq m_{\tilde{g}} \simeq \mu \simeq 500$ GeV; this leads to a gaugino-like LSP, since we assume “gaugino mass unification”, i.e. $6m_{\tilde{B}} \simeq 3m_{\tilde{W}} \simeq m_{\tilde{g}}$. We also choose a small value for the ratio of vevs, $\tan\beta = 3.6$. We see that the final spectra depend sensitively on the primary X decay products [15], especially in the large x region. This strong dependence on the unknown primary X decay mode(s) should be kept in mind when one is trying to quantitatively test “top-down”

models. Nevertheless, we can make a few general statements about these results. To that end we first analyze ratios of FFs of the different stable particles divided by the FF of the same initial particle into protons. Recall that these FFs directly represent the flux at source if X undergoes two-body decay.

Taking the ratios of the different FFs renders some features more evident, as can be seen from figs. 3 and 4. First of all, in the low x region most FFs show the same power law behavior, and the ratios become quite independent of the initial particle. The exceptions are the FFs into the LSP and ν_τ . This comes from the fact that the LSP flux as well as most of the ν_τ are produced in the perturbative cascade above 1 TeV and in the following decays of the heavy particles of the spectrum; they receive no contribution from the decays of light hadrons, although the ν_τ flux receives a minor contribution from the decay of b -flavored hadrons. In contrast, at low x the fluxes of ν_e , ν_μ , e and γ all dominantly originate from the decays of light hadrons, in particular of charged or neutral pions; we saw in fig. 2 that the shape of the light hadron spectrum at small x is essentially determined by the perturbative QCD evolution, i.e. is independent of the initial particle I . In the region $x \lesssim 0.01$ we thus predict FFs into ν_μ and γ to be approximately 3 to 4 times larger than the FF into protons, while the FFs into electrons and ν_e are around twice the FF into protons. The FFs into LSP and ν_τ are five to 20 times smaller than the one into protons. Note that the LSP flux at small x from an initial particle is almost the same as that from its superpartner. It is determined completely by the MSSM cascade, i.e. by the supersymmetric DGLAP equations, and is almost independent of details of the supersymmetric spectrum. However, even at $x = 0.01$ the FF into the LSP does retain some sensitivity to the start of the cascade, i.e. to the initial particle I and hence to the primary X decay mode(s).

At larger values of x the ratios of the FFs depend more and more strongly on the initial particle. As $x \rightarrow 1$ the proton flux is always orders of magnitude smaller than the fluxes of all other stable particles. One reason is that the proton is a composite particle, i.e. its FF contains a convolution with a non-perturbative factor which falls as a power of $1 - x$ at large x . Even before this convolution the flux of partons (quarks and gluons) that can give rise to protons is suppressed at large x due to copious emission of (soft) gluons, whereas the FFs into leptons, photons and LSPs can remain large at large x . If the progenitor I of the cascade is a strongly interacting superparticle, at large x the FF into the LSP always dominates over the other FFs. For an initial quark or gluon, the flux of γ (which is the second after LSP for a squark or gluino) will dominate at large x . On the contrary, in the case of an initial lepton, W , B or H_i , the strongest fluxes will be leptonic ones, the exact order depending of the initial particle. Moreover, for an initial (s)lepton, the fluxes will be significantly higher at high x (and hence smaller at low x , because of energy conservation) than for strongly interacting (super)particles or Higgs bosons. Finally, an initial B or \tilde{B} has a δ -peak at $x = 1$ (not visible in the figures) in D_B^γ and $D_{\tilde{B}}^{\text{LSP}}$, respectively, in addition to a smooth component that vanishes as $x \rightarrow 1$. This behavior reflects the inability of B or \tilde{B} to radiate a boson, i.e. there are no splitting processes $B \rightarrow B + X$ or $\tilde{B} \rightarrow \tilde{B} + X$.

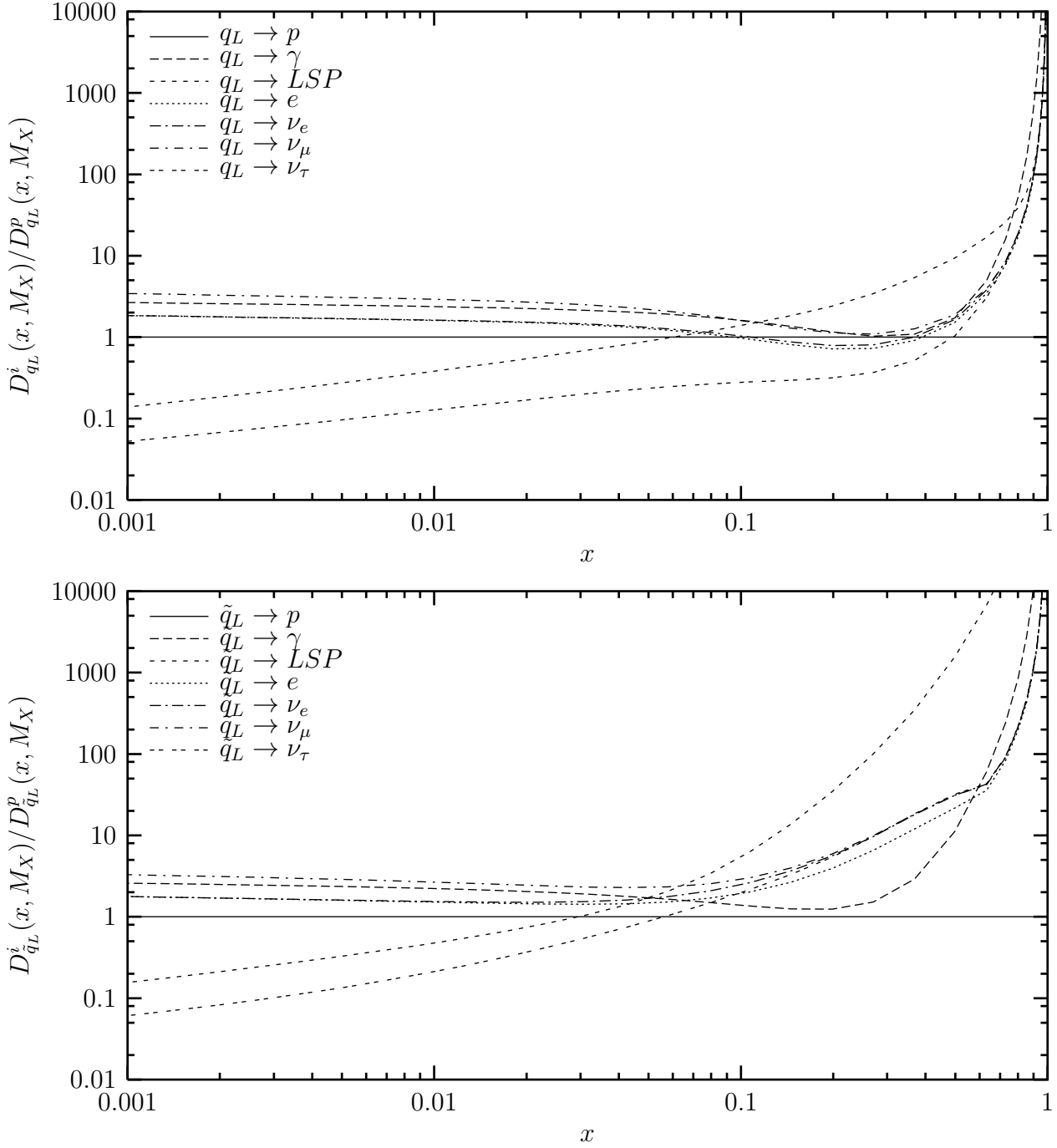


Figure 3: Ratios of FFs D_I^h/D_I^p for different stable particles h , for an initial first or second generation $SU(2)$ doublet quark, $I = q_L$, (top) or squark, $I = \tilde{q}_L$ (bottom).

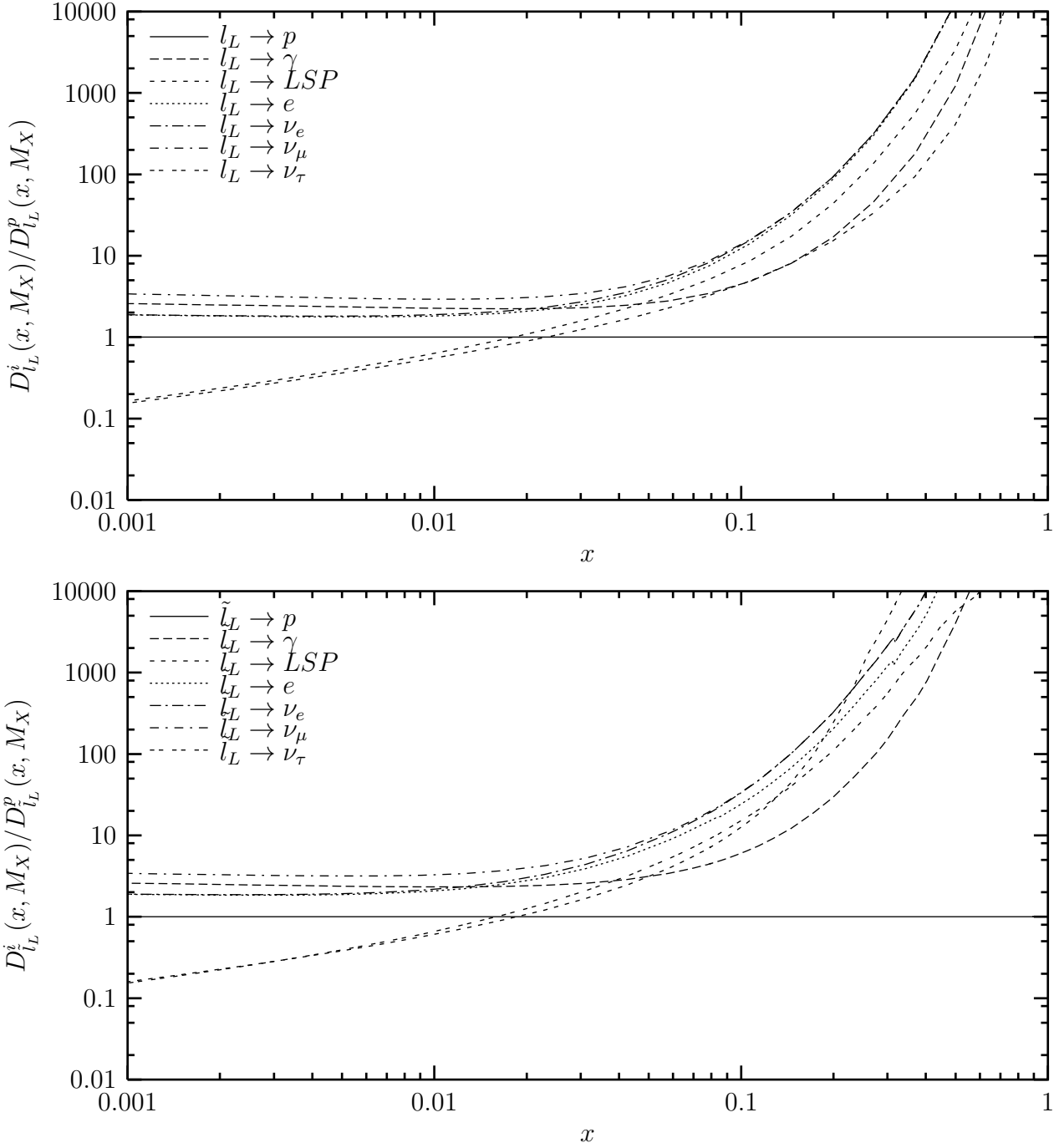


Figure 4: As in fig. 3, but for initial first or second generation $SU(2)$ doublet lepton, $I = l_L$, (top) or slepton, $I = \tilde{l}_L$ (bottom).

init (s)part → energy [%] ↓	q_L	\tilde{q}_L	u_R	\tilde{u}_R	d_R	\tilde{d}_R	t_L	\tilde{t}_L	t_R	\tilde{t}_R	b_R	\tilde{b}_R
p	10.0	8.3	9.1	7.0	11.5	8.4	9.3	8.0	8.8	7.8	10.3	8.1
γ	22.9	19.1	25.2	19.1	24.1	18.0	20.5	17.8	22.0	19.0	22.0	18.0
LSP	5.8	17.8	6.4	28.8	6.1	29.1	5.9	17.3	5.6	19.0	4.9	19.1
e	15.7	14.0	15.5	11.7	14.9	11.3	16.5	14.5	16.4	13.9	16.3	14.1
ν_e	15.6	14.0	15.2	11.5	14.7	11.2	16.4	14.5	16.2	13.8	16.1	13.9
ν_μ	28.0	24.2	27.5	20.8	27.8	20.9	27.5	24.1	26.9	23.2	27.9	23.5
ν_τ	1.3	1.8	0.4	0.4	0.3	0.4	3.0	2.9	3.4	2.6	1.6	2.3
sum	99.2	99.2	99.3	99.3	99.2	99.2	99.2	99.2	99.2	99.2	99.1	99.2

Table 1: Energy fractions $\int_0^1 dx x D_I^p(x, M_X^2)$ carried by the stable particles p at the end of the cascade, for initial (s)quarks of the 1st/2nd and 3rd generations. We took $M_X = 10^{16}$ GeV and a sparticle spectrum with gaugino-like LSP, as described in Sec. 3.1.

3.2 Energy distribution between the final stable particles

In the following tables we show the total energy carried per each type of particle at the end of the cascade, depending on the progenitor of the cascade, for the same set of SUSY parameters as in Sec. 3.1. As stated earlier, we are able to verify energy conservation up to at most a few per mille at each step of the cascade, including its very end. We see that the “lost” energy is somewhat larger for (s)squarks, gluons and gluinos than for (s)leptons. This is due to numerical artefacts. The biggest numerical uncertainties arise from the Runge–Kutta method.[‡]

Note that even for an initial quark or gluon, more than 35% of the energy is carried by the electromagnetic channels (electrons plus photons), while neutrinos carry about 40%; in this case most of these fluxes originate from the decays of light hadrons, chiefly pions. The corresponding numbers for superparticles are slightly smaller, the difference being made up by the increased energy fraction carried by the LSP (at large x); an initial $SU(2)$ singlet squark leads to a higher energy fraction in LSPs, since $SU(2)$ singlet sfermions usually decay directly into the LSP, which is Bino-like for our choice of parameters, whereas $SU(2)$ doublet sfermions preferentially decay via a cascade involving $\tilde{\chi}_2^0$ or $\tilde{\chi}_1^\pm$.

Lepton-induced showers have a far smaller photon component, but now an even larger fraction of the energy is carried by electrons and/or neutrinos, while protons carry at most 2%

[‡]For practical reasons, we used a fixed virtuality step in this algorithm, which we had to keep reasonably large, the whole program being already quite time-consuming. In the worst cases, our choice of the virtuality step leads to errors of the order of a few per mille; such a precision is certainly sufficient for our purposes.

initial (s)particle \rightarrow energy fraction (in %) \downarrow	l_L	\tilde{l}_L	e_R	\tilde{e}_R	τ_L	$\tilde{\tau}_L$	τ_R	$\tilde{\tau}_R$
p	1.2	2.2	0.1	0.1	1.2	2.1	0.1	1.0
γ	4.5	6.4	6.1	5.1	10.4	9.6	20.0	11.3
LSP	2.6	28.5	2.0	47.6	2.7	30.5	1.8	36.6
e	29.6	19.2	60.2	31.0	9.1	8.9	14.3	7.1
ν_e	29.6	19.1	15.2	7.9	9.1	8.8	14.1	6.9
ν_μ	31.1	21.9	15.3	8.0	12.9	12.8	19.5	9.8
ν_τ	1.1	2.2	0.1	0.1	54.3	27.1	30.0	27.1
sum	99.8	99.7	99.8	99.8	99.8	99.7	99.8	99.7

Table 2: Energy fractions carried by the stable particles at the end of the cascade, for initial (s)leptons of the 1st/2nd and 3rd generations. Parameters are as in Table 1.

initial (s)particle \rightarrow energy fraction (in %) \downarrow	B	\tilde{B}	W	\tilde{W}	g	\tilde{g}	H_1	\tilde{H}_1	H_2	\tilde{H}_2
p	1.8	1.5	7.3	6.1	9.8	9.1	8.5	7.0	8.0	5.6
γ	71.6	4.1	17.8	14.2	22.5	20.7	19.4	16.7	18.9	14.1
LSP	4.2	76.9	7.0	24.5	8.4	14.0	4.9	18.6	4.9	31.2
e	7.2	5.7	17.0	14.0	15.2	14.4	17.2	14.6	17.1	12.4
ν_e	5.2	4.0	17.4	14.1	15.0	14.2	17.2	14.6	17.5	12.5
ν_μ	7.6	5.9	26.4	21.6	27.1	25.4	27.2	22.9	27.1	19.3
ν_τ	2.1	1.7	6.5	4.9	1.0	1.2	5.1	4.4	6.1	4.2
sum	99.8	99.8	99.4	99.4	99.1	98.9	99.5	98.9	99.5	99.3

Table 3: Energy fractions carried by the stable particles at the end of the cascade, for initial bosons and bosinos. Parameters are as in Table 1.

of the primary’s energy. In this case the difference between an initial particle and its superpartner is much larger than in case of strongly interacting particles, since a much higher fraction of an initial slepton’s energy goes into LSPs, due to the reduced perturbative shower and shorter superparticle decay cascades. This also explains why more than 70% of the energy of an initial B (\tilde{B}) goes into photons (LSPs). The energy fractions for an initial $SU(2)$ gauge or Higgs boson resemble those for a quark (with the exception of an increased ν_τ component, which is however washed out by neutrino oscillations), although the shapes of the corresponding FFs differ quite dramatically. The energy fraction carried by protons is always quite small. Pions are created much more abundantly in the non-perturbative hadronization, and decay into leptons (2/3) and photons (1/3). As noted earlier, this explains the regularity and the features of the small x behavior.

3.3 Dependence on SUSY parameters

As stated in [15], the general features of our results described above depend very little on the set of SUSY parameters we are using. Here we give a more precise analysis of the influence of different parameters describing the SUSY spectrum. As usual we present our results as $x^3 \cdot D_I^p(x, M_X^2)$. The multiplication with the third power of the energy leads to an approximately flat cosmic ray spectrum for $E \lesssim 10^{10}$ GeV [6]. In our case it suppresses the small- x region, leading to maxima in the curves at x between 0.1 and 1.

We first studied the dependence of our results on the overall SUSY mass scale, by comparing results for two different ISASUSY input mass scales for scalars and gluinos: $M_{SUSY} \sim 500$ GeV and 1 TeV. As expected, this change has almost no impact on the final results, since the details of the decay chains of heavy (s)particles will depend mostly on the relative ordering of the (s)particle spectrum (e.g. allowing or preventing some decay modes), rather than on their absolute mass scale. Moreover, a factor 2 or 3 in the scale where the MSSM evolution is terminated does not change the FFs much, since the DGLAP equations describe an evolution which is only logarithmic in the virtuality.

Next we compared two rather extreme values of $\tan \beta$, namely 3.6 and 48, leaving all dimensionful parameters at the weak scale unchanged. Once again the effect is very small. The only visible difference occurs for initial H_1 and \tilde{H}_1 , where the increase of $\tan \beta$ produces more ν_τ at large x , as can be seen in fig. 5. However, flavor oscillations will essentially average the three neutrino fluxes between source and detector, so we expect very little direct dependence of measurable quantities on $\tan \beta$. The main remaining effect is an increase of the overall multiplicity by $\sim 30\%$ for an initial H_1 or \tilde{H}_1 in case of large $\tan \beta$, due to the increased shower activity from the much larger bottom Yukawa coupling. However, the situation could be different in more constrained models, where the spectrum is described by a few soft breaking parameters specified at some high energy scale. In this case a change of $\tan \beta$ generally changes the sparticle and Higgs spectrum, and can also greatly modify some branching ratios.

In order to get a feeling for how the various FFs depend on the relative ordering of the dimensionful parameters describing the SUSY spectrum, we investigated two rather extreme cases. They resemble two qualitatively different regions of parameter space in the minimal su-

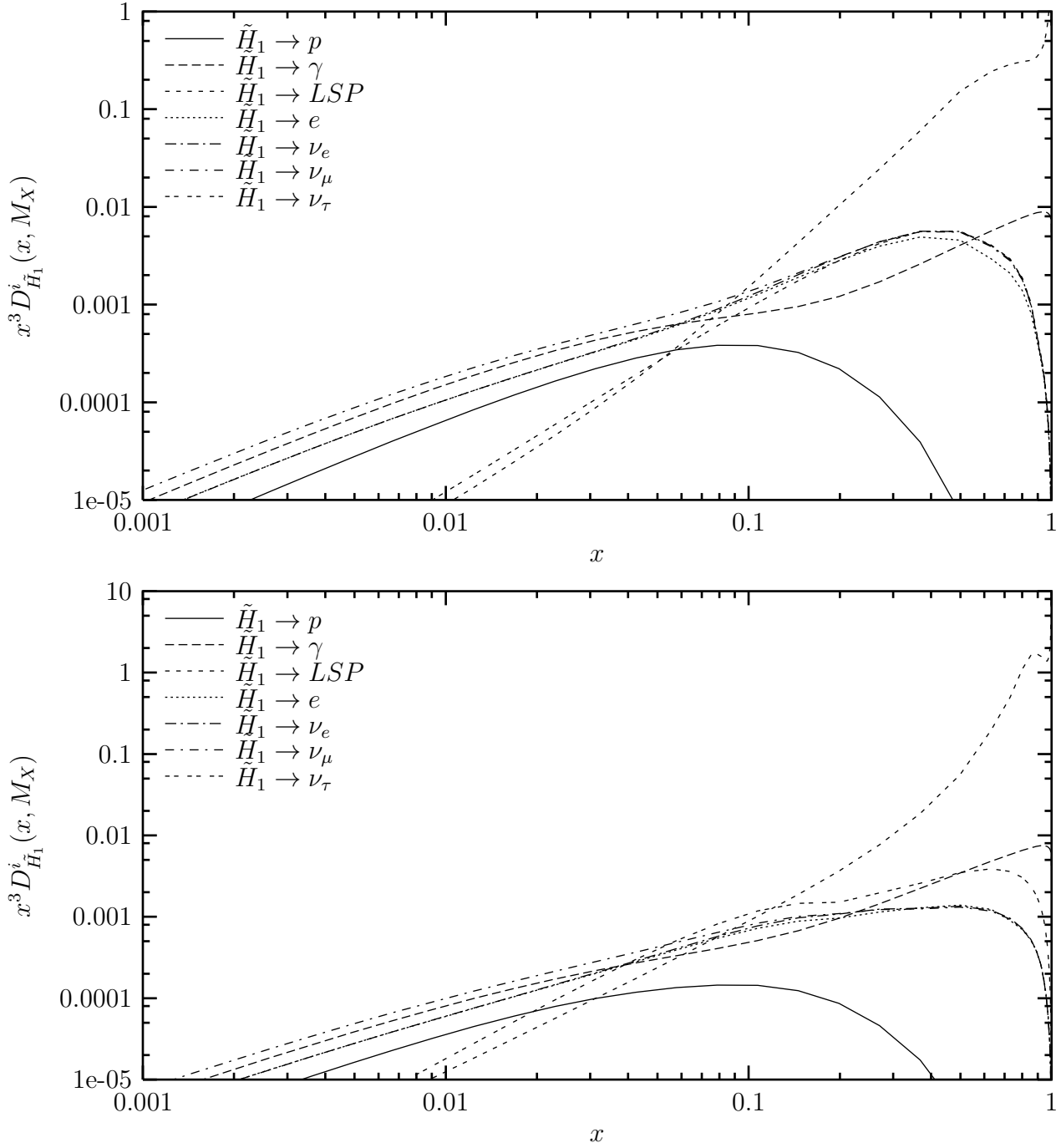


Figure 5: FFs into the final stable particles for an initial \tilde{H}_1 for $\tan\beta = 3.6$ (top) or 48 (bottom).

pergravity (mSUGRA or CMSSM) model where the thermal LSP relic density is acceptably small [36].[§] In the first scenario the LSP $\tilde{\chi}_1^0$ has small mass splitting to the lightest stau, $\tilde{\tau}_1$. We took the following values for the relevant soft breaking parameters: $m_{\tilde{q}} \simeq m_{\tilde{g}} = 1$ TeV for all squarks, $m_{\tilde{l}_L} = 250$ GeV for all $SU(2)$ doublet sleptons, $m_{\tilde{l}_R} \simeq 200$ GeV for $l = e, \mu$ but reduced $m_{\tilde{\tau}_R}$ so that $m_{\tilde{\tau}_1} = m_{\tilde{\chi}_1^0} + 13$ GeV = 163 GeV; note that in mSUGRA one needs large mass splitting between squarks and sleptons if the LSP mass is to be close to the $\tilde{\tau}_1$ mass. The physical sfermion masses receive additional contributions from $SU(2) \times U(1)_Y$ symmetry breaking, and, in case of the third generation, from mixing between singlet and doublet sfermions; in case of \tilde{t} , contributions $+m_t^2$ to the diagonal entries of the mass matrix also have to be added. Our choice $\mu = 1$ TeV together with the assumption of gaugino mass unification ensures that the LSP is an almost pure bino.

In contrast, in the second scenario we took $\mu = -100$ GeV, $m_{\tilde{g}} = 800$ GeV, so that the LSP is dominated by its higgsino components, although the bino component still contributes $\sim 20\%$. In this scenario we took $m_{\tilde{q}} = 1.5$ TeV for all squarks and $m_{\tilde{l}} = 1.2$ TeV for all sleptons, since in mSUGRA large scalar masses are required if the LSP is to have a large higgsino component. We took CP-odd Higgs boson mass $m_A = 1$ TeV in both cases, and $\tan\beta = 3.6$; we just saw that the latter choice is not important for us. In the following we will refer to these two choices as the “gaugino” and “higgsino” set of parameters, respectively.

In Fig. 6 we compare the FFs of an initial first or second generation $SU(2)$ doublet quark q_L for these two scenarios. The main difference occurs in the FF into the LSP, which is significantly softer for the higgsino set. The reason is that most heavy superparticles (sfermions and gluinos) preferentially decay into gaugino-like charginos and neutralinos, which have much larger couplings to most squarks than the higgsino-like states do. These gaugino-like states are the lighter two neutralinos and lighter chargino in case of the gaugino set, but they are the heavier $\tilde{\chi}$ states for the higgsino set. The supersymmetric decay chains therefore tend to be longer for the higgsino set, which means that less energy goes into the LSP produced at the very end of each chain.

Fig. 7 shows the same comparison for an initial first or second generation $SU(2)$ doublet squark \tilde{q}_L . Not surprisingly, the FFs of a squark are more sensitive to details of the sparticle spectrum than those of a quark. In particular, in addition to the reduced FF into the LSP, we now also see that the FFs into neutrinos and electrons are suppressed for the higgsino set relative to the gaugino set. This is partly again due to the longer decay chains, which pushes these FFs towards smaller x where the x^3 normalization factor suppresses them more strongly, and partly because the branching ratios for leptonic decays of the $SU(2)$ gaugino-like $\tilde{\chi}$ states are smaller here than for the gaugino set, which implies that fewer leptons are produced in sparticle decays. On the other hand, the longer decay chains and larger hadronic branching ratios for $\tilde{\chi}$ decays characteristic of the higgsino set lead to an increase of the total multiplicity of 25% or so, as can be seen from the FFs at small x ; of course, in this region the ratios of these FFs again approach their universal values, as discussed in Sec. 3.1.

[§]In our case X particles could contribute significantly to the Dark Matter; in this scenario, which is realized only for a small region of the total allowed M_X, τ_X plane, the upper bound on the LSP relic density would have to be tightened accordingly, but the allowed regions of parameter space would be qualitatively the same.

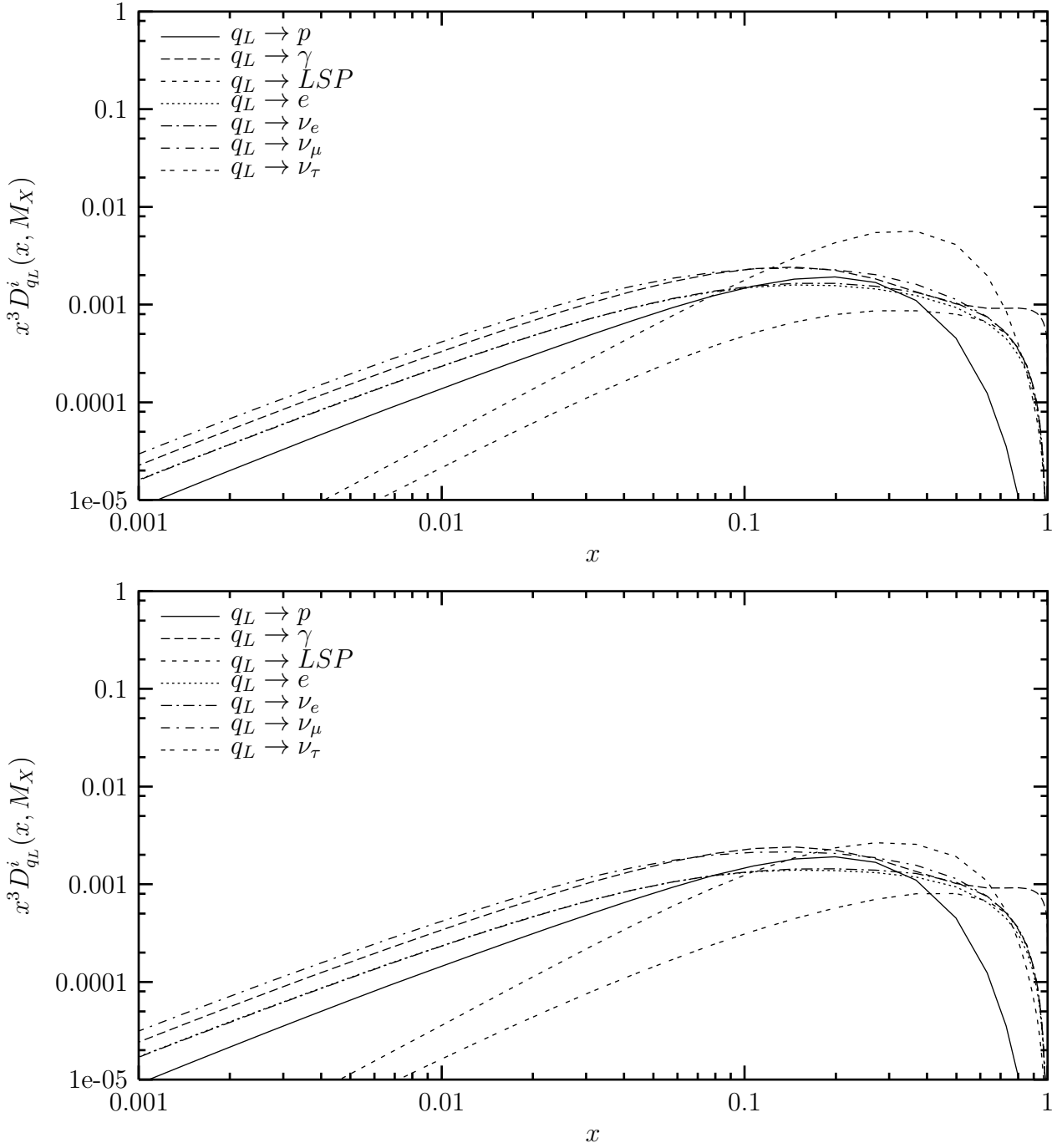


Figure 6: FFs into the final stable particles for an initial $SU(2)$ doublet quark of the first or second generation q_L , for the gaugino (top) and higgsino (bottom) set of parameters.

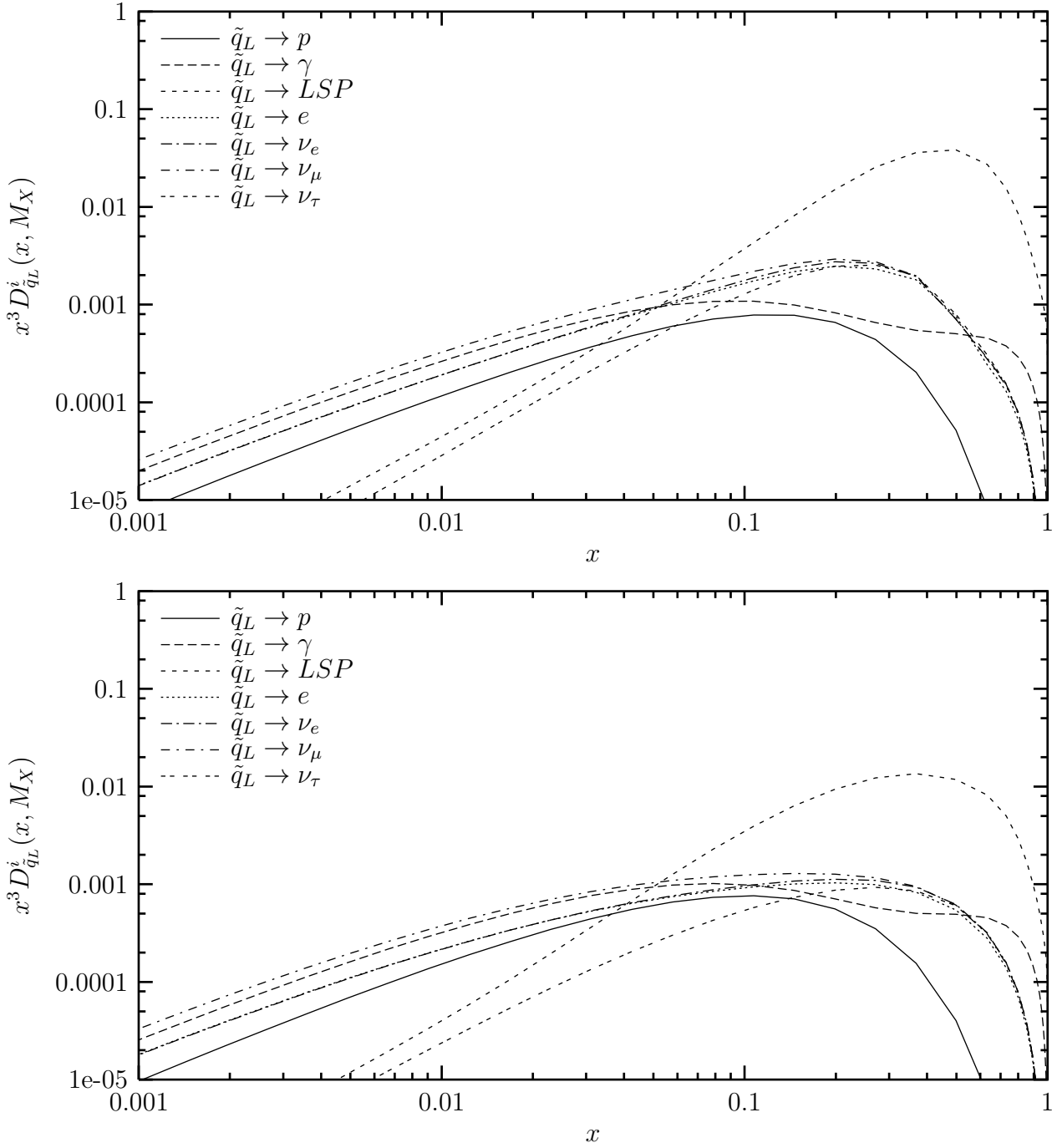


Figure 7: FFs into the final stable particles for an initial $SU(2)$ doublet squark of the first or second generation \tilde{q}_L , for the gaugino (top) and higgsino (bottom) set of parameters.

If the initial particle is strongly interacting, the rapid evolution of the shower ensures that the generalized FFs (11) describing the evolution between M_{SUSY} and M_X essentially vanish at $x \simeq 1$, i.e. all spectra are smooth. In contrast, if the initial particle I has only weak interactions, a significant δ -peak will remain at $x = 1$ in the generalized FF \tilde{D}_I^I . If I is a superparticle or Higgs boson, the decays of I can therefore lead to sharp edges in the final FFs. This is illustrated in Fig. 8, which shows the FFs for an initial first or second generation $SU(2)$ doublet sleptons \tilde{l}_L . The parameters of the gaugino set are chosen such that \tilde{l}_L sleptons can only decay into $l + \text{LSP}$. The decays of the \tilde{l}_L which survive at $x = 1$ therefore lead to edges in the FFs into e, ν_e and ν_μ ; recall that \tilde{l}_L is an equal mixture of $\tilde{e}_L, \tilde{\nu}_e, \tilde{\mu}_L$ and $\tilde{\nu}_\mu$. The edge in the FF into e occurs at a somewhat larger value of x than those in the FFs into $\nu_{e,\mu}$, since after $SU(2)$ symmetry breaking the charged members of the slepton doublets are a little heavier than the neutral ones; the decay $\tilde{e}_L \rightarrow e\tilde{\chi}_1^0$ therefore deposits more energy in the electron than $\tilde{\nu}_e \rightarrow \nu_e\tilde{\chi}_1^0$ deposits in the neutrino. However, in both cases the bulk of the energy goes into the LSP, which is rather close in mass to the slepton. This is quite different for the higgsino set, where sleptons are much heavier than all $\tilde{\chi}$ states. As a result, almost the entire slepton energy can go into the decay lepton, leading to FFs into e, ν_e and ν_μ that are peaked very near $x = 1$ (after multiplying with x^3). Furthermore, since most sleptons now first decay into heavier $\tilde{\chi}$ states rather than directly into $\tilde{\chi}_1^0$, the FF into the LSP is much softer than for the gaugino set. Finally, the effect of the longer decay chains of SUSY particles on the overall multiplicity now amounts to about a factor of 2, and is thus much more pronounced than for initial squarks; this can be explained by the reduced importance of the shower evolution in case of only weakly interacting primaries.

Fig. 9 shows that in case of an initial H_1 Higgs doublet, the role of the two parameter sets is in some sense reversed. Recall that we chose $\tan\beta > 1$ and $m_A \gg M_Z$. In that case the heavy Higgs bosons mostly consist of various components of the H_1 doublet, with only small admixtures of H_2 ; see eq.(B.1) in Appendix B. As usual with only weakly interacting primaries, the generalized FF $D_{H_1}^{H_1}$ remains sizable at $x = 1$ even at scale M_X . In the higgsino set, the dominant decay modes of the heavy Higgs bosons involve a gaugino and a higgsino, leading to a large FF into the LSP in this case. Since in the gaugino set the mass of the higgsino-like $\tilde{\chi}$ states is very close to the mass of the heavy Higgs bosons, these supersymmetric decay modes are closed for the heavy Higgs bosons in this case, which instead predominantly decay into top quarks, with decays into b quarks and τ leptons also playing some role. The fragmentation and decay products of these heavy quarks lead to a significantly larger FF into protons in the gaugino region; semi-leptonic t and b decays as well as the τ decays also lead to enhanced FFs into electrons and neutrinos for the gaugino set. Finally, the hadronic showers initiated by the decay products of the top quarks as well as by the b quarks produced directly in the decays of Higgs bosons raise the total multiplicity for the gaugino set to a value which is slightly larger than that for the higgsino set.

As final example we compare the FFs of an initial \tilde{H}_2 higgsino doublet in Fig. 10. Here we again find a larger FF into the LSP for the higgsino set, including a peak at $x = 1$. In this case this is simply a reflection of the large \tilde{H}_2^0 component of the LSP. On the other hand, in case of the gaugino set \tilde{H}_2 projects almost exclusively into the heavier $\tilde{\chi}$ states, which have many two-

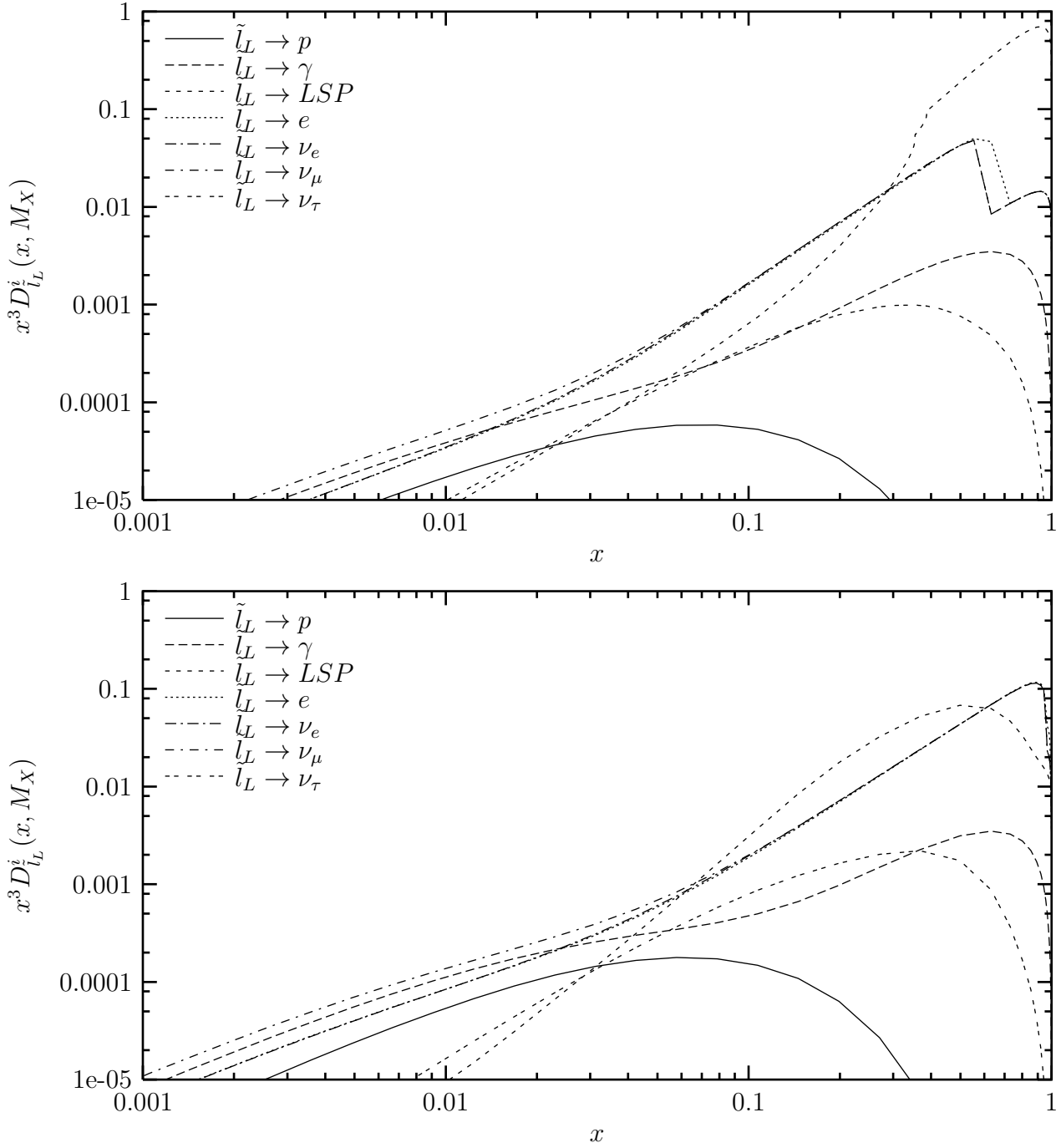


Figure 8: FFs into the final stable particles for an initial $SU(2)$ doublet slepton of the first or second generation \tilde{l}_L , for the gaugino (top) and higgsino (bottom) set of parameters.

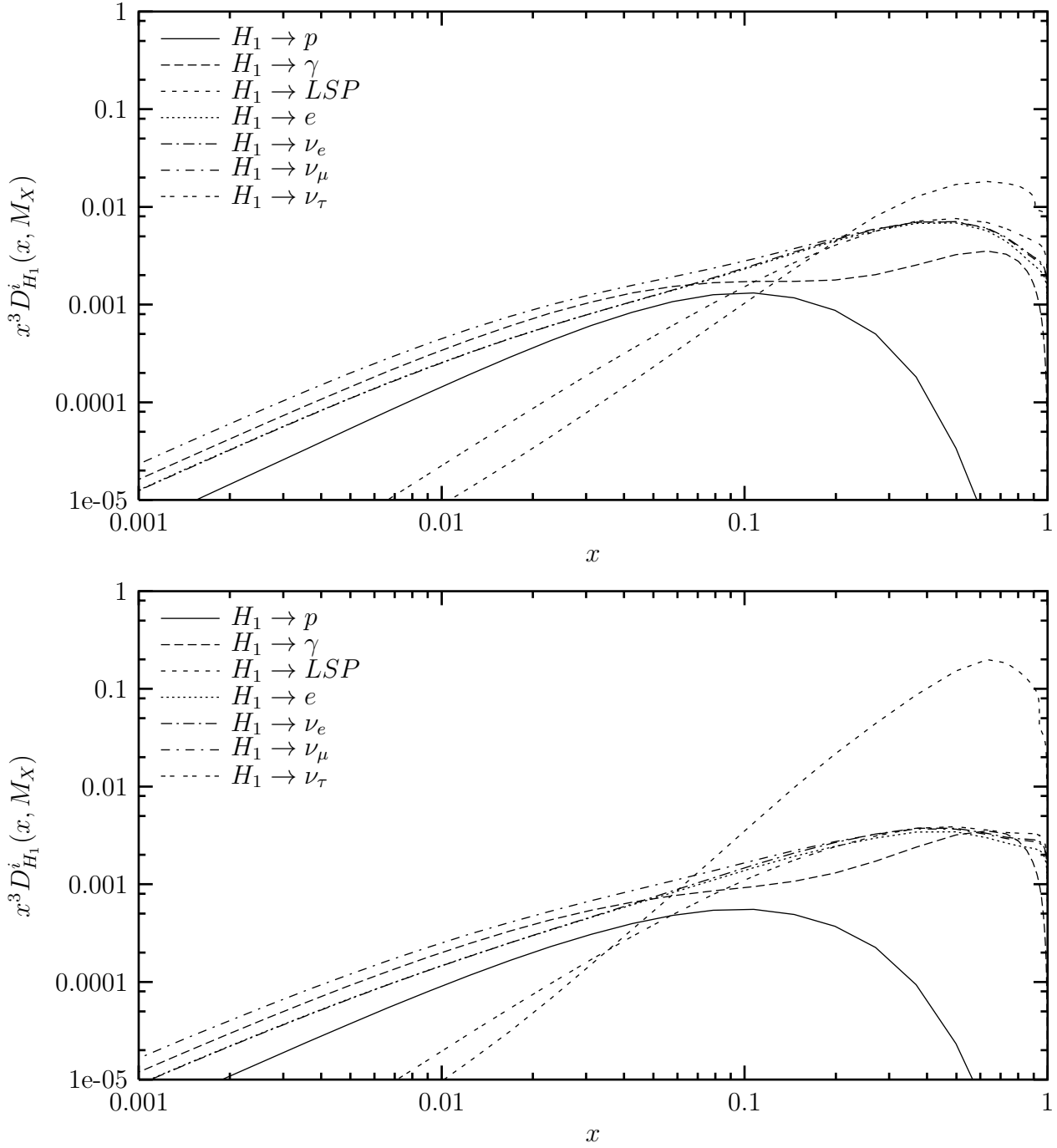


Figure 9: FFs into the final stable particles for an initial H_1 Higgs doublet, for the gaugino (top) and higgsino (bottom) set of parameters.

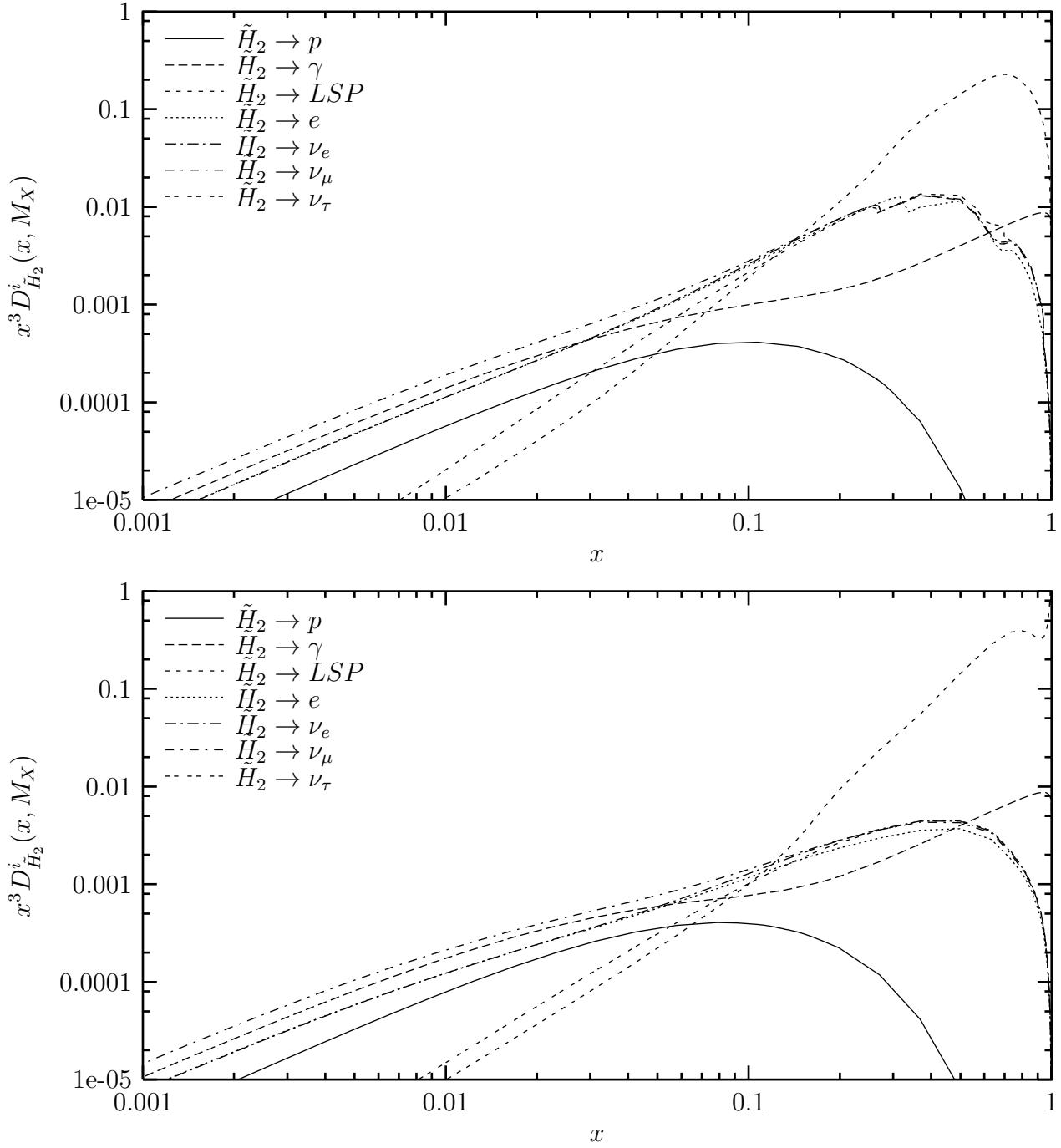


Figure 10: FFs into the final stable particles for an initial \tilde{H}_2 higgsino doublet, for the gaugino (top) and higgsino (bottom) set of parameters.

body decay modes into sleptons and leptons. This explains the relative enhancement at large x of the FFs into leptons that we observe for the gaugino set, as well as the structures in these FFs. On the other hand, the longer sparticle decay chains again imply a somewhat larger overall multiplicity for the higgsino set. These decays of heavy sparticles are important here since the large top Yukawa coupling of \tilde{H}_2 initiates a significant parton shower in this case, where numerous superparticles are produced. This is quite different for an initial \tilde{H}_1 at small $\tan\beta$ (not shown), where we find a *smaller* overall multiplicity for the higgsino set, since the number of produced superparticles remains small, and the initial particle \tilde{H}_1 has a longer decay chain for the gaugino set.

Altogether we see that the SUSY spectrum can change the final FFs, and thus the final spectra of X decay products, significantly. Generally this effect is stronger for an initial superparticle or heavy Higgs boson than for an SM particle, and stronger for only weakly interacting particles than for those with strong interactions. However, with the exception of the FFs into the LSP, the variation is usually not more than a factor of two, and often much less. The dependence of the X decay spectra on SUSY parameters can therefore be significant for detailed quantitative analyses, but this dependence is always weaker than the dependence on the primary X decay mode(s).

3.4 Coherence effects at small x : the MLLA solution

So far we have used a simple power law extrapolation of the hadronic (non-perturbative) FFs at small x . This was necessary since the original input FFs of ref.[25] are valid only for $x \geq 0.1$. As noted earlier, we expect our treatment to give a reasonable description at least for a range of x below 0.1. However, at very small x , color coherence effects should become important [32]. These lead to a flattening of the FFs, giving a plateau in $xD(x)$ at $x_{\text{plateau}} \sim \sqrt{Q_{\text{had}}/M_X} \sim 10^{-8}$ for $M_X = 10^{16}$ GeV. One occasionally needs the FFs at such very small x . For example, the neutrino flux from X decays begins to dominate the atmospheric neutrino background at $E \sim 10^5$ GeV [37, 38], corresponding to $x \sim 10^{-11}$ for our standard choice $M_X \sim 10^{16}$ GeV. In this subsection we therefore describe a simple method to model color coherence effects in our FFs.

This is done with the help of the so-called limiting spectrum derived in the modified leading log approximation. The key difference to the usual leading log approximation described by the DGLAP equations is that QCD branching processes are ordered not towards smaller virtualities of the particles in the shower, but towards smaller emission angles of the emitted gluons; note that gluon radiation off gluons is the by far most common radiation process in a QCD shower. This angular ordering is due to color coherence, which in the conventional scheme begins to make itself felt only in NLO (where the emission of two gluons in one step is treated explicitly). It changes the kinematics of the parton shower significantly. In particular, the requirement that emitted gluons still have sufficient energy to form hadrons strongly affects the FFs at small x . For sufficiently high initial shower scale and sufficiently small x the MLLA evolution equations can be solved explicitly in terms of a one-dimensional integral [32]. This essentially yields the modified FF describing the perturbative gluon to gluon fragmentation, \tilde{D}_g^g in the language of

eq.(10). In order to make contact with experiment, one makes the additional assumption that the FFs into hadrons coincide with \tilde{D}_g^g , up to an unknown constant; this goes under the name of “local parton–hadron duality” (LPHD) [33]. Here we use the fit of this “limiting spectrum” in terms of a distorted Gaussian [39], which (curiously enough) seems to describe LEP data on hadronic FFs somewhat better than the “exact” MLLA prediction does. It is given by

$$F_i(\xi, \tau) \equiv x D_i(x, Q) = \frac{\bar{n}_i}{\sigma\sqrt{2\pi}} \exp\left[\frac{1}{8}k + \frac{1}{2}s\delta - \frac{1}{4}(2+k)\delta^2 + \frac{1}{6}s\delta^3 + \frac{1}{24}k\delta^4\right], \quad (18)$$

where \bar{n}_i is the average multiplicity. The other quantities appearing in eq.(18) are defined as follows:

$$\begin{aligned} \tau &= \log \frac{Q}{\Lambda}, \\ \xi &= \log \frac{1}{x}, \\ \bar{\xi} &= \frac{1}{2}\tau \left(1 + \frac{\rho}{24}\sqrt{\frac{48}{\beta\tau}}\right) + \mathcal{O}(1), \\ \sigma &= \langle(\xi - \bar{\xi})^2\rangle^{1/2} = \sqrt{\frac{1}{3}} \left(\frac{\beta}{48}\right)^{1/4} \tau^{3/4} \left(1 - \frac{1}{64}\sqrt{\frac{48\beta}{\tau}}\right) + \mathcal{O}(\tau^{-1/4}), \\ \delta &= \frac{\xi - \bar{\xi}}{\sigma}, \\ s &= \frac{\langle(\xi - \bar{\xi})^3\rangle}{\sigma^3} = -\frac{\rho}{16}\sqrt{\frac{3}{\tau}} \left(\frac{48}{\beta\tau}\right)^{1/4} + \mathcal{O}(\tau^{-5/4}), \\ k &= \frac{\langle(\xi - \bar{\xi})^4\rangle}{\sigma^4} = -\frac{27}{5\tau} \left(\sqrt{\frac{1}{48}\beta\tau} - \frac{1}{24}\beta\right) + \mathcal{O}(\tau^{-3/2}). \end{aligned} \quad (19)$$

where β is the coefficient in the one–loop beta–function of QCD and $\rho = 11 + 2N_f/27$, N_f being the number of active flavors. Eqs.(18) and (19) have been derived in the SM, where $\beta = 11 - 2N_f/3$. Following ref.[40] we assume that it remains valid in the MSSM, with $\beta = 3$ above the SUSY threshold M_{SUSY} and $\rho = 11 + 8/9$. Note that we do not attempt to model the transition from the full MSSM to standard QCD here; indeed, we do not know of an easy way to do this, since the limiting spectrum cannot be written as a convolution of two other spectra. On the other hand, the position $\bar{\xi}$ of the plateau depends only on $\sqrt{\beta}$, and only via the second term, which is suppressed by a factor $\sqrt{\tau} \sim 6.5$, whereas the parameters σ and s describing the behavior in the vicinity of the maximum depend in leading order in τ only on $\beta^{1/4}$. Finally, the coefficient ρ is very similar in the SM and MSSM. We therefore expect the error we make by ignoring the transition from MSSM to SM to be smaller than the inherent accuracy of eq.(18).

When comparing MLLA predictions with experiments, the overall normalization \bar{n}_i (which depends on energy) is usually taken from data. We cannot follow this approach here, since no data with $Q \sim M_X$ are available. Moreover, usually MLLA predictions are compared with

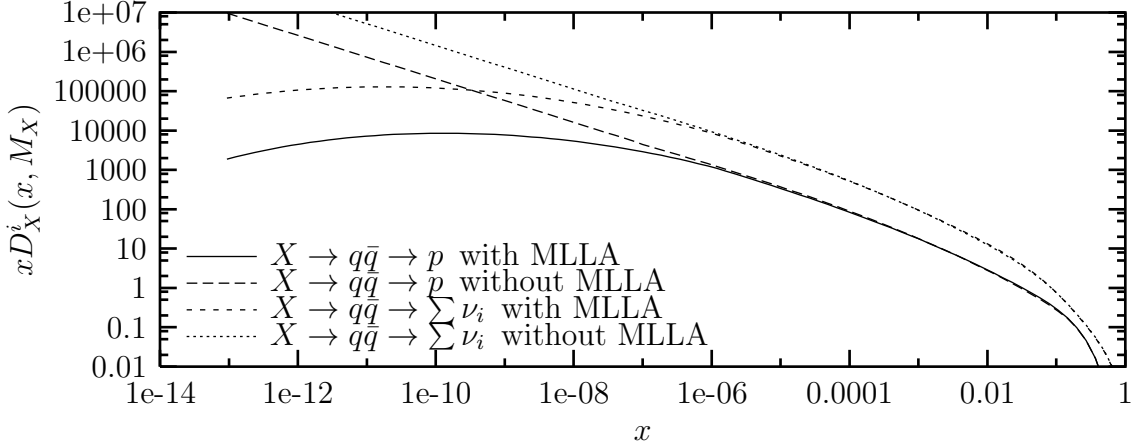


Figure 11: Comparison between the MLLA solution and our results without coherence effects, for the final proton and neutrino spectra. We assume that X undergoes two-body decay into $q_L \bar{q}_L$.

inclusive spectra of all (charged) particles. We need separate predictions for various kinds of hadrons, and are therefore forced to make the assumption that all these FFs have the same x -dependence at small x . This is perhaps not so unreasonable; we saw above that the DGLAP evolution predicts such a universal x -dependence at small x . We then match these analytic solutions (18), (19) with the hadronic FFs D_f^h we obtained from DGLAP evolution and our input FFs at values x_0^h , where for each hadron species h the matching point x_0^h and the normalization \bar{n}_h are chosen such that the FF and its first derivative are continuous; we typically find $x_0 \sim 10^{-4}$. Note that this matching no longer allows to respect energy conservation exactly. However, since the MLLA solution begins to deviate from the original FFs only at $x \sim 10^{-7}$, the additional “energy losses” are negligible.

Some results of our MLLA treatment are shown in Fig. 11. Here the “non-MLLA” curves have been obtained by extrapolating our numerical results described earlier, which extend “only” to $x = 10^{-7}$, by using simple power-law fits. We see that at $x \sim 10^{-11}$ the FFs are suppressed by about two orders of magnitude, but the effect diminishes quickly at larger values of x . Note that the FFs into protons and into neutrinos have slightly different shapes in the small- x region. By assumption the FFs have the same shape for all *hadrons*; however, in going from the spectrum of pions and kaons to the neutrino spectrum, several additional convolutions are required, which shift the peak of the distribution to even smaller values of x . This figure also shows that the MLLA predictions closely tracks the non-MLLA solution for x values that are several orders of magnitude smaller than the matching point x_0 ; this illustrates the advantage of requiring both the FF and its first derivative to be continuous at x_0 .

4 Summary and Conclusions

In this article, we presented a detailed analysis of the decay of a very massive X particle, extending our earlier work [15]. In particular, we were able to improve the accuracy of our code; as a result, we can now ensure energy conservation to a numerical accuracy of better than 1%, as compared to up to several % in ref.[15]. Moreover, we showed that the dependence of our results on the necessary extrapolation of the measured fragmentation functions (FFs) towards small x is negligible. We also included leading higher-order QCD corrections at very small x using the MLLA approximation for taking into account color coherence effects; this approximation is in good agreement with data from particle colliders. These effects become significant for $x \lesssim 10^{-7}$, decreasing the predicted fluxes at $x \sim 10^{-11}$ by about two orders of magnitude.

Furthermore, we showed that varying SUSY parameters can have some impact on our results, affecting the shapes of the FFs at $x \geq 0.01$ and in some cases also the total multiplicity; however, the dependence on the SUSY spectrum is much milder than the dependence on the primary X decay mode(s). Qualitatively the photon and LSP fluxes are the most important ones at large x if the primary is a strongly interacting (s)particle; if the primary has only weak interactions, the lepton fluxes can also be very large at large x . The proton flux is always subdominant in this region. In contrast, the shapes of most FFs at small x can be predicted almost uniquely. This leads to the following ordering of the fluxes at $x < 0.01$: the largest flux is of muon neutrinos, followed by photons, ν_e and electrons, and finally protons. The ratios of these fluxes become almost independent of x in this region, the proton flux being about a factor of five smaller than the ν_μ flux. On the other hand, the two smallest fluxes at small x , of LSPs and finally ν_τ , do depend sensitively on various currently unknown parameters. Generically they rise less rapidly with decreasing x than the other fluxes do; already at $x \sim 10^{-3}$, the ν_τ and LSP flux are usually about one order of magnitude below the proton flux.

Finally, in the appendices we give additional details of our description of the complete cascade. In particular, Appendix A contains the first complete set of leading order splitting functions for the MSSM, including all gauge as well as third generation Yukawa interactions. A “catalogue” containing an almost complete set of FFs for a given set of parameters is given in Appendix E.

This work presents the to date most accurate and complete description of the spectra at source of stable particles resulting from the decay of a superheavy X particle. These spectra are needed for all quantitative tests of the “top-down” explanation of the most energetic cosmic ray events. Of course, in order to be able to compare with fluxes measured on or near Earth, effects due to the propagation through the galactic, and perhaps extragalactic, medium [6] have to be included, which depend on the distribution of X particles throughout the Universe; we have made no attempt to do this. On the other hand, our description of X decays is model-independent in the sense that it allows to incorporate any primary X decay mode. Indeed, it could with very little modification also be used to describe the evolution of very energetic jets produced through some other mechanism (e.g. the annihilation of very massive stable particles), as long as the initial virtuality of the produced particles is comparable to their energy.

Returning to the original problem of ultra-high energy cosmic rays (UHECR), the biggest obstacle towards a test of generic top-down models is the strong dependence of the predicted decay spectra on the primary decay mode. Most previous investigations assumed that X decays into a pair of quarks, but we are not aware of any compelling argument why this should be the dominant decay mode. On the other hand, data may already rule out some classes of top-down models. For example, it seems likely that few, if any, UHECR are photons [41]. In the context of top-down models, this leaves protons as only choice. Our results then seem to disfavor models where X decays primarily into particles with only weak interactions, since this implies a large ratio of the photon to proton flux at large x . However, this argument may not apply if $M_X \gtrsim 10^{13}$ GeV, since then all events seen so far are at $x \lesssim 0.01$, where the ratio of photon to proton fluxes is essentially independent of the primary X decay modes. Moreover, the photon flux may be diminished more efficiently between source and detector than the proton flux. Searches for very energetic neutrinos might therefore lead to somewhat more robust tests of top-down models [37, 38]; as noted earlier, the predicted neutrino flux should begin to exceed the background from atmospheric neutrinos at very small values of x . Nevertheless, the need to normalize the expected flux to the observed flux of UHECR events, and hence to the proton and perhaps photon flux at much larger x , re-introduces a large model dependence even in this case [38]. Moreover, other proposed explanations of the UHECR also predict sizable neutrino fluxes at very high energy, e.g. due to the GZK process itself. The failure to observe such neutrinos could therefore exclude top-down models (given sufficiently large detectors), but a positive signal may not be sufficient to distinguish them from generic “bottom-up” models. This discrimination might be achieved by searching for the predicted flux of very energetic LSPs, since the LSP flux in bottom-up models is undetectably small; however, this test will require very large detectors [42]. We conclude that ultimately the test of this idea will probably require a combined analysis of different signals, at quite different energies and in different detectors. We provide one of the tools needed to perform such an analysis, since we are able to systematically study the fluxes of *all* stable particles at source, and their correlations, for *all* top-down models.

Acknowledgements

We would like to thank Willy van Neerven for helpful comments on higher order corrections. This work was supported in part by the SFB375 of the Deutsche Forschungsgemeinschaft.

Appendix A: Splitting functions of the MSSM

The splitting function (SF) $P_{ji}(x)$ describes the radiation of particle j off particle i . Its x -dependence is determined by the Lorentz structure of the corresponding vertex, while the normalization also depends on the associated group [color and $SU(2)$] factors. If there is no vertex relating these two particles the SF is simply 0. We first list the functional forms we will need, together with the spins of the particles involved in the branching process $i \rightarrow j + k$ (V

for vector, F for spin-1/2 fermion, S for scalar):

$$\begin{aligned}
(0) & \delta(1-x), \\
(1) & i = F, j = F, k = V : \frac{1+x^2}{(1-x)_+}, \\
(2) & i = F, j = V, k = F : \frac{1+(1-x)^2}{x}, \\
(3) & i = F, j = S : k = F : x, \\
(4) & i = F, j = F, k = S : (1-x), \\
(5) & i = S, j = F, k = F : 1, \\
(6) & i = S, j = V, k = S : \frac{2(1-x)}{x}, \\
(7) & i = S, j = S, k = V : \frac{2x}{(1-x)_+}, \\
(8) & i = V, j = F, k = F : (1-x)^2 + x^2, \\
(9) & i = V, j = V, k = V : 2 \left[\frac{1-x}{x} + x(1-x) + \frac{x}{(1-x)_+} \right], \\
(10) & i = V, j = S, k = S : 2x(1-x).
\end{aligned} \tag{A.1}$$

For convenience, we also define $(1') = (1) + (0)$ and $(7') = (7) + (0)$.

α_S	$i = q$	\tilde{q}	g	\tilde{g}
$j = q$	$\frac{4}{3} (1')$	$\frac{4}{3} (5)$	$\frac{N_q}{2} (8)$	$\frac{N_q}{2} (4)$
\tilde{q}	$\frac{4}{3} (3)$	$\frac{4}{3} (7')$	$\frac{N_q}{2} (10)$	$\frac{N_q}{2} (3)$
g	$\frac{4}{3} (2)$	$\frac{4}{3} (6)$	$3 \left[(9) + \left(\frac{3}{2} - \frac{F}{6} \right) (0) \right]$	$3 (2)$
\tilde{g}	$\frac{4}{3} (4)$	$\frac{4}{3} (5)$	$3 (8)$	$3 \left[(1) + \left(\frac{3}{2} - \frac{F}{6} \right) (0) \right]$

Table 4: SUSY-QCD splitting functions P_{ji} , where j and i determine the row and column of the table, respectively. The functional forms denoted by (n) , $n = 0, \dots, 10$ have been defined in eq.(A.1), with $(1') = (1) + (0)$ and $(7') = (7) + (0)$. The “multiplicity factors” are: $N_{t_R} = N_{b_R} = 1$, $N_{t_L} = N_{u_R} = N_{d_R} = 2$ and $N_{q_L} = 4$. In the MSSM phase, i.e. for $Q > M_{\text{SUSY}}$, the number of active flavors (quarks and squarks) is $F = 6$.

The 16 SFs of SUSY-QCD listed in table 4 are derived from [27]; in eq.(14) they come with a factor of the strong coupling α_S . Note that in ref.[27] the chirality index L, R was always summed over; e.g. $P_{t_g} = P_{t_L g} + P_{t_R g}$, where t_L now *only* describes the left-handed top quark (and not the third generation quark doublet). Since these two terms are equal,

one has $P_{t_L g} = P_{t_R g} = P_{qg}/2$. On the other hand, our “(s)quark” distributions always include anti(s)quarks. This re-introduces a factor of 2, so that for us e.g. $P_{t_R g} = P_{qg}$ of [27]. Additional factors arise for (s)quarks of the first and second generation. As described in Sec. 2.2, we always average over (s)quarks and anti(s)quarks with given hypercharge of the first two generations. This implies $P_{u_R g} = P_{d_R g} = 2P_{qg}$ and $P_{q_L g} = 4P_{qg}$, where the additional factor of two in the second expression comes from summing over the $SU(2)$ index of the doublet q_L . The same factors appear in SFs describing gluon to squark splitting as well as gluino splitting into a squark and a quark. A complete list of these factors N_q is given in the table caption. On the other hand, in the absence of flavor-changing interactions SFs involving quarks and squarks only always come with factor 1 if the “compound particles” u_R, q_L etc. are properly normalized.

The SFs stemming from electroweak interactions have similar structures; we just need to compute the correct group and multiplicity factors. The results are listed in tables 5 and 6. In these tables we list SFs including the appropriate multiplicity factor; a single $SU(2)$ doublet *without* antiparticles would have $N_f = 1/2$. Note that there is no difference between Higgs and $SU(2)$ doublet lepton superfields as far as gauge interactions are concerned. Finally, due to the absence of self-interactions of $U(1)$ gauge bosons, the splitting functions P_{BB} and $P_{\tilde{B}\tilde{B}}$ are pure delta-functions, with coefficients fixed by energy conservation, eq.(6). In all three gauge interactions we find that the coefficient of the δ -function is the same in P_{ff} and $P_{\tilde{f}\tilde{f}}$ for any matter fermion f , and also in P_{VV} and $P_{\tilde{V}\tilde{V}}$ for a gauge boson V ; this latter coefficient is $-1/2$ times the coefficient in the β -function of the corresponding gauge coupling.

$g_2 = e/\sin\theta_W$	$i = W$	\tilde{W}	f_L	\tilde{f}_L
$j = W$	$2 \left[(9) + \left(\frac{3}{2} - \frac{N_d}{8} \right) (0) \right]$	2 (2)	$\frac{3}{4}$ (2)	$\frac{3}{4}$ (6)
\tilde{W}	2 (8)	$2 \left[(1) + \left(\frac{3}{2} - \frac{N_d}{8} \right) (0) \right]$	$\frac{3}{4}$ (4)	$\frac{3}{4}$ (5)
f_L	$\frac{N_f}{2}$ (8)	$\frac{N_f}{2}$ (4)	$\frac{3}{4}$ (1')	$\frac{3}{4}$ (5)
\tilde{f}_L	$\frac{N_f}{2}$ (10)	$\frac{N_f}{2}$ (3)	$\frac{3}{4}$ (3)	$\frac{3}{4}$ (7')

Table 5: $SU(2)$ splitting functions P_{ji} , where particles j and i are associated with the row and column, respectively. The functional forms denoted by (n) , $n = 0, \dots, 10$ have been defined in eq.(A.1), with $(1') = (1) + (0)$ and $(7') = (7) + (0)$. N_d is the total number of $SU(2)$ doublets; in the MSSM, $N_d = 14$. f stands for any matter or Higgs fermion, with N_f being the number of doublets (not counting anti-doublets) described by f_L or \tilde{f}_L . For our “compound” states, these are: $N_{q_L} = 6$, $N_{t_L} = 2$, $N_{t_L} = 3$, $N_{\tau_L} = N_{H_1} = N_{H_2} = 1$.

Finally, Yukawa couplings only appear in $H f_L f_R$, $\tilde{h} \tilde{f}_L f_R$ and $\tilde{h} f_L \tilde{f}_R$ vertices. We therefore only need functional forms (3), (4) and (5) from eq.(A.1). The coefficients can be determined from the analogous terms due to $U(1)_Y$ interactions by replacing $(g_Y Y_f)^2$ by $\lambda_f^2/2$, where the extra factor of $1/2$ corrects for the factor $\sqrt{2}$ appearing in front of gaugino-fermion-sfermion

$g_Y = e/\cos\theta_W$	$i = B$	\tilde{B}	f	\tilde{f}
$j = B$	$-\frac{1}{2}\sum_f Y_f^2 (0)$	0	$Y_f^2 (2)$	$Y_f^2 (6)$
\tilde{B}	0	$-\frac{1}{2}\sum_f Y_f^2 (0)$	$Y_f^2 (4)$	$Y_f^2 (5)$
f	$n_f Y_f^2 (8)$	$n_f Y_f^2 (4)$	$Y_f^2 (1')$	$Y_f^2 (5)$
\tilde{f}	$n_f Y_f^2 (10)$	$n_f Y_f^2 (3)$	$Y_f^2 (3)$	$Y_f^2 (7')$

Table 6: $U(1)_Y$ splitting functions P_{ji} , where particles j and i are associated with the row and column, respectively. The functional forms denoted by (n) , $n = 0, \dots, 10$ have been defined in eq.(A.1), with $(1') = (1) + (0)$ and $(7') = (7) + (0)$. The sum of squared hypercharges of all particles $\sum_f Y_f^2 = 11$ in the MSSM. f stands for any matter or Higgs fermion with hypercharge Y_f , while n_f is the number of degrees of freedom (not counting anti-particles) described by f or \tilde{f} . For our “compound” states, these are: $Y_{q_L}^2 = 1/36, n_{q_L} = 12$; $Y_{u_R}^2 = 4/9, n_{u_R} = 6$; $Y_{d_R}^2 = 1/9, n_{d_R} = 6$; $Y_{l_L}^2 = 1/4, n_{l_L} = 4$; $Y_{l_R}^2 = 1, n_{l_R} = 2$; $Y_{t_L}^2 = 1/36, n_{t_L} = 6$; $Y_{t_R}^2 = 4/9, n_{t_R} = 3$; $Y_{b_R}^2 = 1/9, n_{b_R} = 3$; $Y_{\tau_L}^2 = Y_{H_1}^2 = Y_{H_2}^2 = 1/4, n_{\tau_L} = n_{H_1} = n_{H_2} = 2$; $Y_{\tau_R}^2 = 1, n_{\tau_R} = 1$.

λ_f	$i = H$	\tilde{H}	f_L	\tilde{f}_L	f_R	\tilde{f}_R
$j = H$	$-\frac{N_c}{2} (0)$	0	$\frac{1}{2} (3)$	0	(3)	0
\tilde{H}	0	$-\frac{N_c}{2} (0)$	$\frac{1}{2} (4)$	$\frac{1}{2} (5)$	(4)	(5)
f_L	$\frac{N_c}{2} (5)$	$\frac{N_c}{2} (4)$	$-\frac{1}{2} (0)$	0	(4)	(5)
\tilde{f}_L	0	$\frac{N_c}{2} (3)$	0	$-\frac{1}{2} (0)$	(3)	0
f_R	$\frac{N_c}{2} (5)$	$\frac{N_c}{2} (4)$	$\frac{1}{2} (4)$	$\frac{1}{2} (5)$	-1 (0)	0
\tilde{f}_R	0	$\frac{N_c}{2} (3)$	$\frac{1}{2} (3)$	0	0	-1 (0)

Table 7: Splitting functions P_{ji} originating from Yukawa interactions, where particles j and i are associated with the row and column, respectively. The functional forms denoted by (n) , $n = 0, 3, 4, 5$ have been defined in eq.(A.1). Since we only include Yukawa interactions for the third generation, we only have to consider three cases. For the top Yukawa coupling, $f_L = t_L, f_R = t_R, H = H_2$ and number of colors $N_c = 3$; for the bottom Yukawa coupling, $f_L = t_L, f_R = b_R, H = H_1$ and $N_c = 3$; finally, for the tau Yukawa coupling, $f_L = \tau_L, f_R = \tau_R, H = H_1$ and $N_c = 1$.

vertices in the supersymmetric Lagrangian. Since Yukawa interactions couple matter fields with different chiral indices all diagonal SFs due to Yukawa couplings are pure δ -functions, the coefficients again being determined by energy conservation; as before, we find equal coefficients for diagonal SFs of a particle and its superpartner. The resulting SFs are listed in table 7. As usual, these SFs are multiplied with $\alpha_f/(2\pi) \equiv \lambda_f^2/(8\pi^2)$ in the DGLAP equations. The three interactions we consider, involving the top, bottom and tau Yukawa couplings, can all be treated using table 7, by identifying the matter and Higgs fields appropriately and using the correct color factors, as explained in the caption. The $SU(2)$ factors, which lead to the factor of 2 difference between SFs describing radiation off $SU(2)$ singlet or doublet (s)fermions, are the same in all three cases.[†]

Appendix B: Unitary transformations between current and mass eigenstates in the MSSM

In this Appendix we describe the unitary transformations occurring during the SUSY and $SU(2) \otimes U(1)$ breaking, where the quarks, leptons, weak gauge bosons and Higgs bosons as well as all superparticles acquire their masses [43]. The superscript b denotes the mass eigenstates of the broken theory. The fields in the unbroken theory are the same as those described in Sec. 2.2. For example, q_L stands for all left-handed quarks and antiquarks of the two first generations, i.e. the $SU(2)$ doublets (u_L, d_L) , (c_L, s_L) and their antiparticles (\bar{u}_L, \bar{d}_L) , (\bar{c}_L, \bar{s}_L) , and thus describes eight degrees of freedom (times three, if color is counted separately). Similarly, l_L stands for both $SU(2)$ doublets (e_L, ν_e) and (μ_L, ν_μ) and their antiparticles $(\bar{e}_L, \bar{\nu}_e)$ and $(\bar{\mu}_L, \bar{\nu}_\mu)$. On the other hand, u^b only describes u -quarks and their antiparticles, but includes both chirality states, and thus describes four degrees of freedom (not counting color). Recall that the transformation between mass and current eigenstates in eq.(15) only affects the *upper* index of the (generalized) FFs. In the given context q_L therefore stands for the sum, not the average, of its “constituent fields”, as discussed in Sec. 2.2. Recall finally that massive gauge bosons “eat” Goldstone modes from the Higgs sector. These considerations lead to the following transformations for SM fields and Higgs bosons:

$$\begin{aligned} u^b &= c^b = \frac{1}{4} q_L + \frac{1}{2} u_R, \\ d^b &= s^b = \frac{1}{4} q_L + \frac{1}{2} d_R, \\ b^b &= \frac{1}{2} t_L + b_R, \\ t^b &= \frac{1}{2} t_L + t_R, \end{aligned}$$

[†]Strictly speaking, H_1 can only split into τ_R and $\bar{\tau}_L$, not into τ_L and $\bar{\tau}_R$, while the antiparticle H_1^* can only split into τ_L and $\bar{\tau}_R$; analogous remarks hold for the other Yukawa-induced branching processes. However, this distinction plays no role for us, since we always average or sum over particle and antiparticle.

$$\begin{aligned}
e^b &= \mu^b = \frac{1}{4} l_L + \frac{1}{2} e_R, \\
\tau^b &= \frac{1}{2} \tau_L + \tau_R, \\
\nu_e^b &= \nu_\mu^b = \frac{1}{4} l_L, \\
\nu_\tau^b &= \frac{1}{2} \tau_L, \\
g^b &= g, \\
W^b &:= W^+ + W^- = 2 \left(\frac{1}{3} W + \cos^2 \beta \frac{H_1}{4} + \sin^2 \beta \frac{H_2}{4} \right), \\
Z^b &= \sin^2(\theta_W) B + \cos^2(\theta_W) \frac{W}{3} + \cos^2 \beta \frac{H_1}{4} + \sin^2 \beta \frac{H_2}{4}, \\
\gamma^b &= \cos^2(\theta_W) B + \sin^2(\theta_W) \frac{W}{3}, \\
h^{0b} &= \sin^2 \alpha \frac{H_1}{4} + \cos^2 \alpha \frac{H_2}{4}, \\
H^{0b} &= \cos^2 \alpha \frac{H_1}{4} + \sin^2 \alpha \frac{H_2}{4}, \\
A^{0b} &= \sin^2 \beta \frac{H_1}{4} + \cos^2 \beta \frac{H_2}{4}, \\
H^b &:= H^+ + H^- = 2 \left(\sin^2 \beta \frac{H_1}{4} + \cos^2 \beta \frac{H_2}{4} \right). \tag{B.1}
\end{aligned}$$

All superparticles also acquire masses at this stage, and the particles with identical quantum numbers mix together to give the mass eigenstates:

$$\begin{aligned}
\tilde{q}_{L/R}^b &= \tilde{q}_{L/R} \text{ for } q = u, d, s, c, \\
\tilde{b}_1^b &= \frac{1}{2} \cos^2(\theta_b) \tilde{t}_L + \sin^2(\theta_b) \tilde{b}_R, \\
\tilde{t}_1^b &= \frac{1}{2} \cos^2(\theta_t) \tilde{t}_L + \sin^2(\theta_t) \tilde{t}_R, \\
\tilde{b}_2^b &= \frac{1}{2} \sin^2(\theta_b) \tilde{t}_L + \cos^2(\theta_b) \tilde{b}_R, \\
\tilde{t}_2^b &= \frac{1}{2} \sin^2(\theta_t) \tilde{t}_L + \cos^2(\theta_t) \tilde{t}_R, \\
\tilde{e}_L^b &= \tilde{\mu}_L^b = \frac{1}{4} \tilde{l}_L, \\
\tilde{e}_R^b &= \tilde{\mu}_R^b = \frac{1}{2} \tilde{e}_R, \\
\tilde{\tau}_1^b &= \frac{1}{2} \cos^2(\theta_\tau) \tilde{\tau}_L + \sin^2(\theta_\tau) \tilde{\tau}_R, \\
\tilde{\tau}_2^b &= \frac{1}{2} \sin^2(\theta_\tau) \tilde{\tau}_L + \cos^2(\theta_\tau) \tilde{\tau}_R,
\end{aligned}$$

$$\begin{aligned}
\tilde{\nu}_e^b &= \tilde{\nu}_\mu^b = \frac{1}{4} \tilde{l}_L, \\
\tilde{\nu}_\tau^b &= \frac{1}{2} \tilde{\tau}_L, \\
\tilde{g}^b &= \tilde{g}, \\
\tilde{\chi}_1^b &:= \tilde{\chi}_1^+ + \tilde{\chi}_1^- = \left[\sin^2(\gamma_R) + \sin^2(\gamma_L) \right] \frac{\tilde{W}}{3} + \cos^2(\gamma_R) \frac{\tilde{H}_2}{2} + \cos^2(\gamma_L) \frac{\tilde{H}_1}{2}, \\
\tilde{\chi}_2^b &:= \tilde{\chi}_2^+ + \tilde{\chi}_2^- = \left[\cos^2(\gamma_R) + \cos^2(\gamma_L) \right] \frac{\tilde{W}}{3} + \sin^2(\gamma_R) \frac{\tilde{H}_2}{2} + \sin^2(\gamma_L) \frac{\tilde{H}_1}{2}, \\
\tilde{\chi}_i^{0b} &= \left| v_1^{(i)} \right|^2 \frac{\tilde{H}_1}{2} + \left| v_2^{(i)} \right|^2 \frac{\tilde{H}_2}{2} + \left| v_3^{(i)} \right|^2 \frac{\tilde{W}}{3} + \left| v_4^{(i)} \right|^2 \tilde{B}.
\end{aligned} \tag{B.2}$$

Here we have largely followed the notation of ISASUSY [24]. However, we have used the more common symbol $\tilde{\chi}$ for charginos and neutralinos; in ISASUSY notation, $\tilde{\chi}_1^b = \tilde{W}_-$, $\tilde{\chi}_2^b = \tilde{W}_+$, and $\tilde{\chi}_i^{0b} = \tilde{Z}_i$. The mixing angles α (in the Higgs sector), $\theta_b, \theta_t, \theta_\tau$ (in the sfermion sector), γ_L, γ_R (in the chargino sector) as well as the $v_i^{(j)}$ (in the neutralino sector) have been computed numerically using ISASUSY.

Appendix C: Two- and three-body decay spectra

Generalities

We want to define the decay functions (DFs) \tilde{P}_{sS} describing two- or three-body decay $S \rightarrow s$, see eq.(16). These DFs can be obtained directly from the decay spectrum of S in the ultra-relativistic limit, where the energy E_S is much larger than the mass M of S :

$$\tilde{P}_{sS}(z) = \frac{1}{\Gamma} \frac{d\Gamma(E_S)}{dz}, \tag{C.1}$$

where $z = E_s/E_S$. This spectrum can e.g. be evaluated by first computing the double differential decay distribution $d^2\Gamma/(dE_s^* d\cos\theta^*)$ in the *rest frame* of S , then boosting the four-momentum of s with boost factor $\gamma = E_S/M$ at angle θ^* relative to \vec{p}_s , and finally integrating over $\cos\theta^*$ subject to the constraint that the boosted energy of s equals E_s . Note that eq.(C.1) implies $\int_0^1 \tilde{P}_{sS}(z) dz = 1$; if S -decays produce N identical particles s , the corresponding \tilde{P}_{sS} would thus have to be multiplied with an extra factor of N , in order to correctly reproduce the total multiplicity in the final state. Finally, momentum conservation implies $\sum_s \int_0^1 z \tilde{P}_{sS}(z) = 1$.

In case of two-body decays $S \rightarrow i+j$ the energy E_s^* in the rest frame of S is fixed completely by the kinematics. The boost and integration over $\cos\theta^*$ then leads to a flat decay function:

$$\tilde{P}_{iS}^{(2)}(z) = \left\{ \left[1 - \left(\frac{m_1 + m_2}{M} \right)^2 \right] \left[1 - \left(\frac{m_1 - m_2}{M} \right)^2 \right] \right\}^{-\frac{1}{2}} \Theta(z - z_-^{(i)}) \Theta(z_+^{(i)} - z) \tag{C.2}$$

for the decay product i with $i = 1$ or 2 . The kinematic minimum and maximum $z_{\pm}^{(i)}$ of z are given by:

$$z_{\pm}^{(i)} = \frac{1}{2} \left(1 + \frac{m_i^2 - m_j^2}{M^2} \pm \sqrt{\left[1 - \left(\frac{m_1 + m_2}{M} \right)^2 \right] \left[1 - \left(\frac{m_1 - m_2}{M} \right)^2 \right]} \right). \quad (\text{C.3})$$

For example, for $m_1 \rightarrow M$, $m_2 \rightarrow 0$, eq.(C.3) implies $z_{\pm}^{(1)} \rightarrow 1$, $z_{\pm}^{(2)} \rightarrow 0$, i.e. the entire energy of S goes into the massive decay product. In contrast, for $m_1 = m_2$, the energy of S will on average be shared equally between the two decay products; if $m_1 = m_2 \rightarrow 0$, the $z^{(i)}$ can lie anywhere between zero and one. Since E_s^* is fixed in this case, our treatment of two-body decays is exact up to possible polarization effects; we do not expect these effects to be very important, except perhaps in case of τ decays (which, however, usually do not contribute very much to the final spectra of stable particles).

Three-body decays lead to a nontrivial distribution of the energy of the decay products already in the rest frame of S . For simplicity we assume that at most one of the three decay products is massive; this should be a safe approximation, except for $b \rightarrow c\tau\nu_\tau$ decays, which have a rather small branching ratio. We then need separate DFs for the massive and massless decay products. For the massive decay product, with mass m , we find

$$\tilde{P}_{sS}^{(3)}(z) = N_3 \left[1 - z + \frac{m^2}{M^2} \left(1 - \frac{1}{z} \right) \right] \quad (\text{C.4})$$

where $z \in [\frac{m^2}{M^2}, 1]$ and the normalization factor is given by:

$$N_3 = \left[\frac{1}{2} \left(1 - \frac{m^4}{M^4} \right) + \frac{m^2}{M^2} \log \frac{m^2}{M^2} \right]^{-1}. \quad (\text{C.5})$$

If on the contrary, s is one of the massless decay products, we find:

$$\tilde{P}_{sS}^{(3)}(z) = N_3 \left[1 - z - \frac{m^2}{M^2} \left(1 + \log \frac{M^2}{m^2} + \log(1 - z) \right) \right], \quad (\text{C.6})$$

where now $z \in [0, 1 - \frac{m^2}{M^2}]$; the normalization factor N_3 has been given in eq.(C.5).

Our treatment of three-body decays is not exact, since it ignores dynamical effects (described by the invariant Feynman amplitude) on the decay spectrum in the S rest frame.* However, treating these effects properly is quite nontrivial, since it would force us to introduce many different three-body decay functions. Note in particular that massive superparticles (charginos and neutralinos) do generally not decay via $V - A$ interactions, unlike the b and c quarks and heavy μ and τ leptons in the SM. Moreover, the Feynman amplitudes in many cases depend nontrivially on the polarization of the decaying particle; this could only be described

*The calculation of the corresponding branching ratio in ISASUSY does include these dynamical effects; in other cases the required branching ratio can be taken directly from experiment, e.g. for τ decays.

As mentioned earlier, the leptonic b and c decay products have to be included in the normalization of the FFs D_b^h and D_c^h . To that end, we introduce R_c and R_s , the energy carried by the c and s quark in semi-leptonic b - and c - decays, respectively, as well as x_B and x_D , the energy fraction of the b (c) quark carried by the b -flavored (c -flavored) hadron. The latter are given by

$$x_{B,D} = \int_0^1 z D_{\text{Pet}}^{b,c}(z) dz, \quad (\text{C.7})$$

where $D_{\text{Pet}}^{b,c}$ is the Peterson FF [35] for b and c quarks, respectively; we took $\epsilon_c = 0.15$, $\epsilon_b = 0.015$ for the single free parameter in these FFs. We compute R_c and R_s from pure phase space, i.e. we again ignore possible effects of the Feynman amplitudes on the three-body decay distributions. This gives:

$$\begin{aligned} R_c &= \frac{1}{\overline{m}_b \Gamma(b \rightarrow cl\nu)} \int_{\overline{m}_c}^{E_c, \text{max}} dE_c E_c \frac{d\Gamma(b \rightarrow cl\nu)}{dE_c} \\ &= \frac{(1-r)^3}{3(1-r^2) - 6r \log r}, \end{aligned} \quad (\text{C.8})$$

where $r = \overline{m}_c^2/\overline{m}_b^2 = 0.157$ for our choice of average b - and c -hadron masses; note that $R_c \rightarrow 1/3$ (1) for $r \rightarrow 0$ (1). Eq.(C.8) can also be used for the computation of R_s , with $\overline{m}_c \rightarrow \overline{m}_s \simeq 0.5$ GeV, $\overline{m}_b \rightarrow \overline{m}_c$. The FFs of [25] only include the hadrons produced in the fragmentation and decays of the c - and b -quarks. Their normalization, which we need to know for the necessary extrapolation of these FFs towards small x as discussed in Appendix D, is therefore given by

$$\begin{aligned} \frac{1}{x_B} \sum_h \int_0^1 z D_b^h(z) dz &= \frac{1 - x_B}{x_B} \\ &+ [1 - B_l(b)] \cdot [1 - B_l(c)] \\ &+ B_l(b) \cdot [1 - B_l(c)] \cdot R_c \\ &+ [1 - B_l(b)] \cdot B_l(c) \cdot (R_c \cdot R_s + 1 - R_c) \\ &+ B_l(b) \cdot B_l(c) \cdot R_c \cdot R_s \\ &= \frac{1}{x_B} - B_l(b) \cdot (1 - R_c) - R_c \cdot B_l(c) \cdot (1 - R_s). \end{aligned} \quad (\text{C.9})$$

The right hand side can be understood as follows: the first line describes the contribution of the light hadrons produced when the b -quark hadronizes into a b -flavored hadron; the second line describes purely hadronic decays; the third line describes leptonic primary b decays followed by hadronic c decays (in this case only the fraction R_c of the b -hadrons energy goes into hadrons); the fourth line describes the hadronic energy fraction in the case of a hadronic primary b decay followed by leptonic c -decays; finally, the fifth line describes the hadronic energy fraction after leptonic decays in both the primary and secondary decays. The same holds for c -hadron

decays, up to the simplifying fact that “ s -hadrons” are already fully included into the FFs of [25]. We get:

$$\frac{1}{x_D} \sum_h \int_0^1 z D_c^h(z) dz = \frac{1}{x_D} - B_l(c) + B_l(c) \cdot R_s. \quad (\text{C.10})$$

Appendix D: Parameterization of the input fragmentation functions

Here we give the input fragmentation functions (FFs) we used to describe the hadronization of quarks and gluons, taken from [25], and the parameters of the extrapolation we made in the small x region.

The functions taken from ref [25] are given with the functional form $Nx^\alpha(1-x)^\beta$; there are given in table 8, at the scale where quarks and hadrons hadronize, i.e. $Q_0 = \max(m_q, Q_{had})$. We used the NLO results, excepted for the s quark, for which we had to use the LO ones, because the NLO form didn't allow us to impose energy conservation and continuity at low x .

As we showed in Sec. 2.3, the final result at low x depends very little on the chosen power law in our parameterization

$$f(x) = ax^{-\alpha'} + b \log x + c, \quad a > 0, \quad (\text{D.1})$$

once energy conservation has been imposed. Here we therefore only give results for a parameterization where α' is taken to be 1. That is, we assume that the multiplicity due to non-perturbative effects gets the same contribution for each decade of energy, if the hadron's energy is small compared to that of the initial parton.

In order to obtain a unique solution with the only two constraints at our disposal (energy conservation and continuity of the FFs), we imposed these constraints on the sum of the FFs $\sum_h D_i^h(x, Q^2)$, where i is a given initial parton, and h runs over the final hadrons. Of course, energy will be conserved independently for each initial parton i . For each i we define a cut-off x_0^i which defines the transition between the functions given in [25] and our extrapolation. The x_0^i have to be chosen such that the equations of energy conservation admit a solution; a necessary (but generally not sufficient) requirement is that the integral over the original FFs satisfy $\sum_h \int_{x_0}^1 dz z D_i^h(z) < 1$. Our requirement of continuity at x_0 implies that the final results depend very little on the precise values of the x_0^i . For simplicity we assume that all the $D_i^h(x, Q_{had}^2)$ for a given i have the same shape at small x ; recall that purely perturbative effects ensure that this is true after DGLAP evolution, which anyway greatly reduces the sensitivity to the input. The normalizations for the various hadrons can then be read off directly from the results of ref.[25], once x_0 has been determined. The results are presented in table. 9, which lists the cut-off x_0^i , the coefficients a, b, c of the functional form (D.1) describing the *sum* $\sum_h D_i^h$ for fixed parton i , and the normalization coefficients[†] N_i^h , so that $D_i^h = N_i^h \sum_h D_i^h$; of course, $\sum_h N_i^h = 1 \forall i$.

[†]At first sight the relative ordering of the N_u^K, N_d^K factors may seem counter-intuitive. Indeed, a u -quark

$D_p^h(x, Q_0^2)$ $= Nx^\alpha(1-x)^\beta$	p	n	π^\pm	π^0	K^\pm	K^0
u	$N = 1.26$	0.63	0.448	0.224	0.178	4.96
	$\alpha = 0.0712$	0.0712	-1.48	-1.48	-0.537	0.0556
	$\beta = 4.13$	4.13	0.913	0.913	0.759	2.8
d	0.63	1.26	0.448	0.224	4.96	0.178
	0.0712	0.0712	-1.48	-1.48	0.0556	-0.537
	4.13	4.13	0.913	0.913	2.8	0.759
s	4.08	4.08	22.3	11.15	0.259	0.259
	-0.0974	-0.0974	0.127	0.127	-0.619	-0.619
	4.99	4.99	6.14	6.14	0.859	0.859
c	0.0825	0.0825	6.17	3.085	4.26	4.26
	-1.61	-1.61	-0.536	-0.536	-0.241	-0.241
	2.01	2.01	5.6	5.6	4.21	4.21
b	24.3	24.3	0.259	0.1295	1.32	1.32
	0.579	0.579	-1.99	-1.99	-0.884	-0.884
	12.1	12.1	3.53	3.53	6.15	6.15
g	1.56	1.56	3.73	1.865	0.231	0.231
	0.0157	0.0157	-0.742	-0.742	-1.36	-1.36
	3.58	3.58	2.33	2.33	1.8	1.8

Table 8: Input fragmentation functions at small x , with functional form $Nx^\alpha(1-x)^\beta$, taken from [25] at $Q_0 = \max(m_q, Q_{had})$. We took their NLO results for u,d,c,b and g, but the LO result for the s quark. See the text for further details.

initial parton	x_0	a	b	c	p	n	π^\pm	π^0	K^\pm	K^0
u	0.27	4.06	-9.74	-14.40	0.05	0.025	0.38	0.19	0.05	0.31
d	0.27	4.06	-9.74	-14.40	0.025	0.05	0.38	0.19	0.31	0.05
s	0.20	5.74	-18.47	-31.42	0.14	0.14	0.41	0.21	0.05	0.05
c	0.27	4.06	-4.16	-6.24	0.05	0.05	0.30	0.15	0.22	0.22
b	0.20	5.74	-27.81	-49.27	0.08	0.08	0.35	0.17	0.16	0.16
g	0.37	1.82	-4.81	-2.40	0.05	0.05	0.50	0.25	0.07	0.07

Table 9: Coefficients of the extrapolation of the input fragmentation functions at small x . Column 2 gives the cut-off x_0 where we switch from the FFs from [25] to a parameterization in the form (D.1). Columns 3 to 5 give the coefficients of this parameterization, as applied to the sum $\sum_h D_i^h$. The remaining columns give normalizations N_i^h , so that $D_i^h = N_i^h \sum_h D_i^h$. Note that h always stands for the sum of particle and anti-particle, whenever the two are not identical; for example, π^\pm stands for the sum of π^+ and π^- , K^0 stands for the sum of K^0 and \bar{K}^0 , etc.

Appendix E: Stable particle spectra for different initial (super)particles

Here we give an almost complete set of FFs for different initial particles, for one set of SUSY parameters, with low $\tan\beta$ and gaugino-like LSP; the dependence of these results on the SUSY parameters has been analyzed in Sec. 3.3. We used a ratio of Higgs vevs $\tan\beta = 3.6$, a gluino and scalar mass scale $M_{\text{SUSY}} \sim 500$ GeV, a supersymmetric Higgs mass parameter $\mu = 500$ GeV, a CP-odd Higgs boson mass $m_A = 500$ GeV and trilinear soft breaking parameter $A_t = 1$ TeV. As usual, we plot $x^3 \cdot D_I^P(x, M_X)$. We take $M_X = 10^{16}$ GeV, as appropriate for a GUT interpretation of the X particle.

should more readily fragment into a charged Kaon than into a neutral one, whereas the opposite behavior is expected for d -quarks. Recall, however, that here we are only interested in the behavior at small x . In this case ref.[25] finds the opposite behavior as at large x , i.e. u -quarks indeed seem to be more likely to produce a *soft* neutral kaon than a *soft* charged kaon.

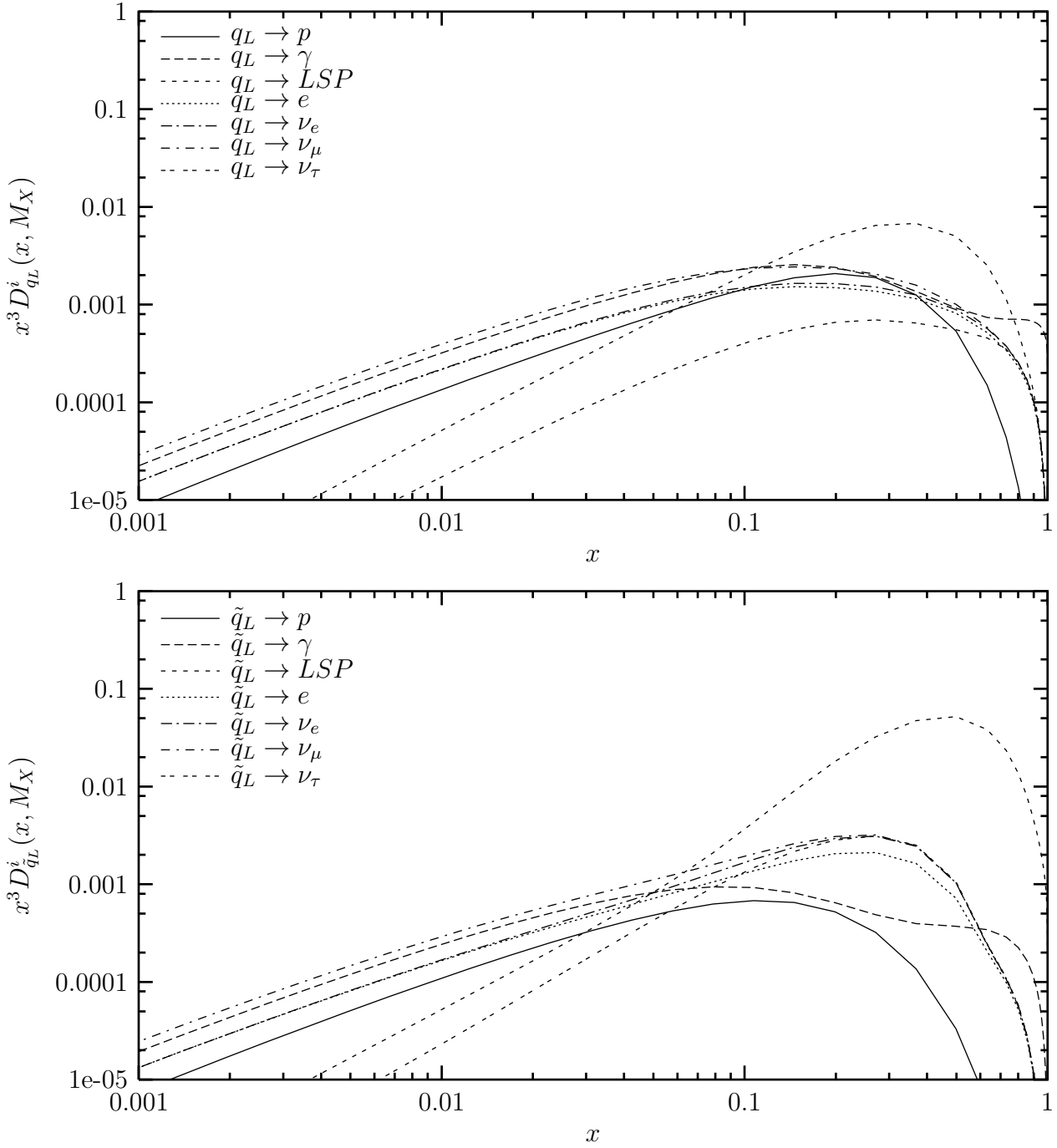


Figure 13: Fragmentation functions of a first or second generation $SU(2)$ doublet quark (top) and a squark (bottom) into stable particles.

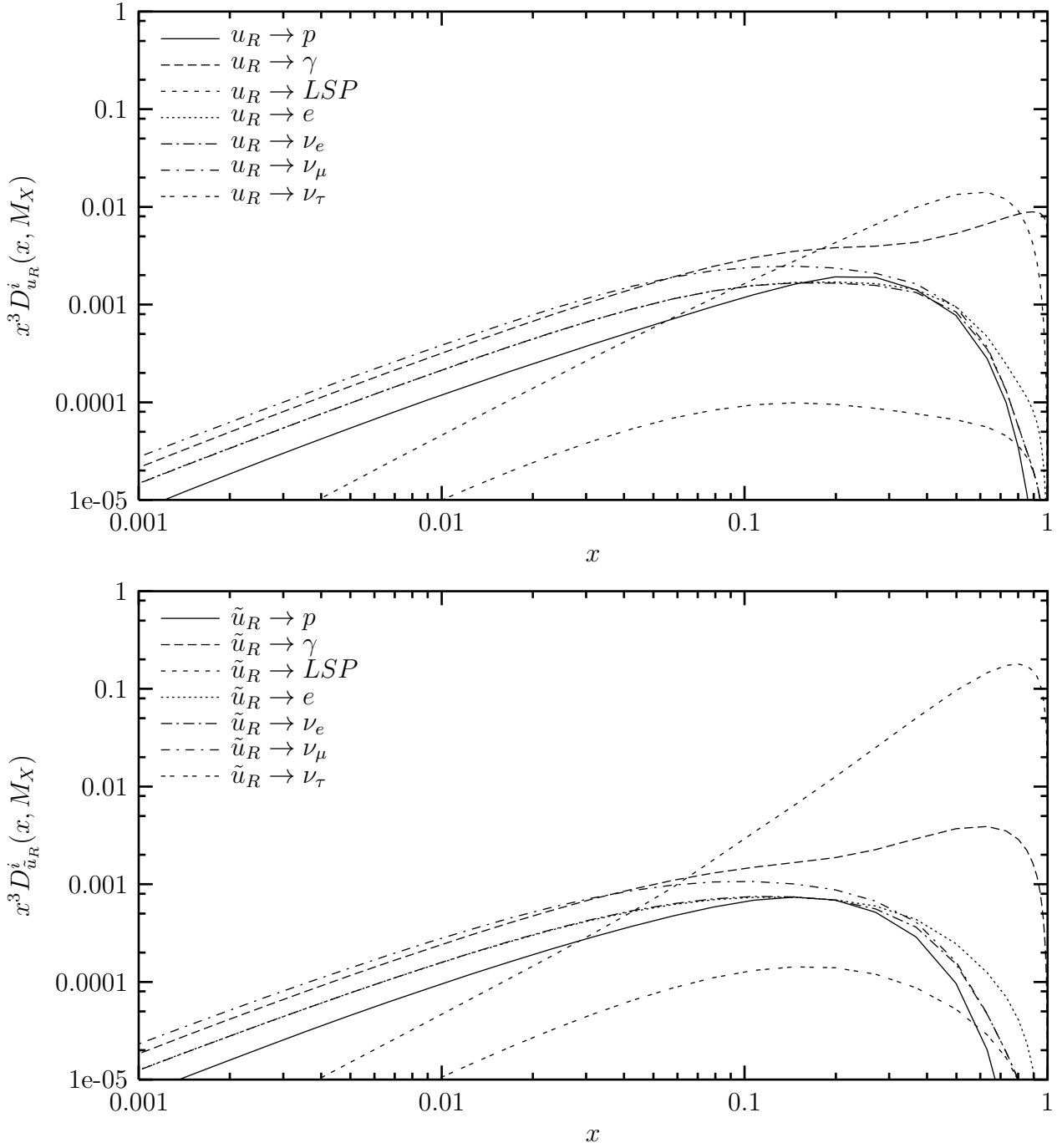


Figure 14: Fragmentation functions of a first or second generation $SU(2)$ singlet quark (top) and a squark (bottom) into stable particles.

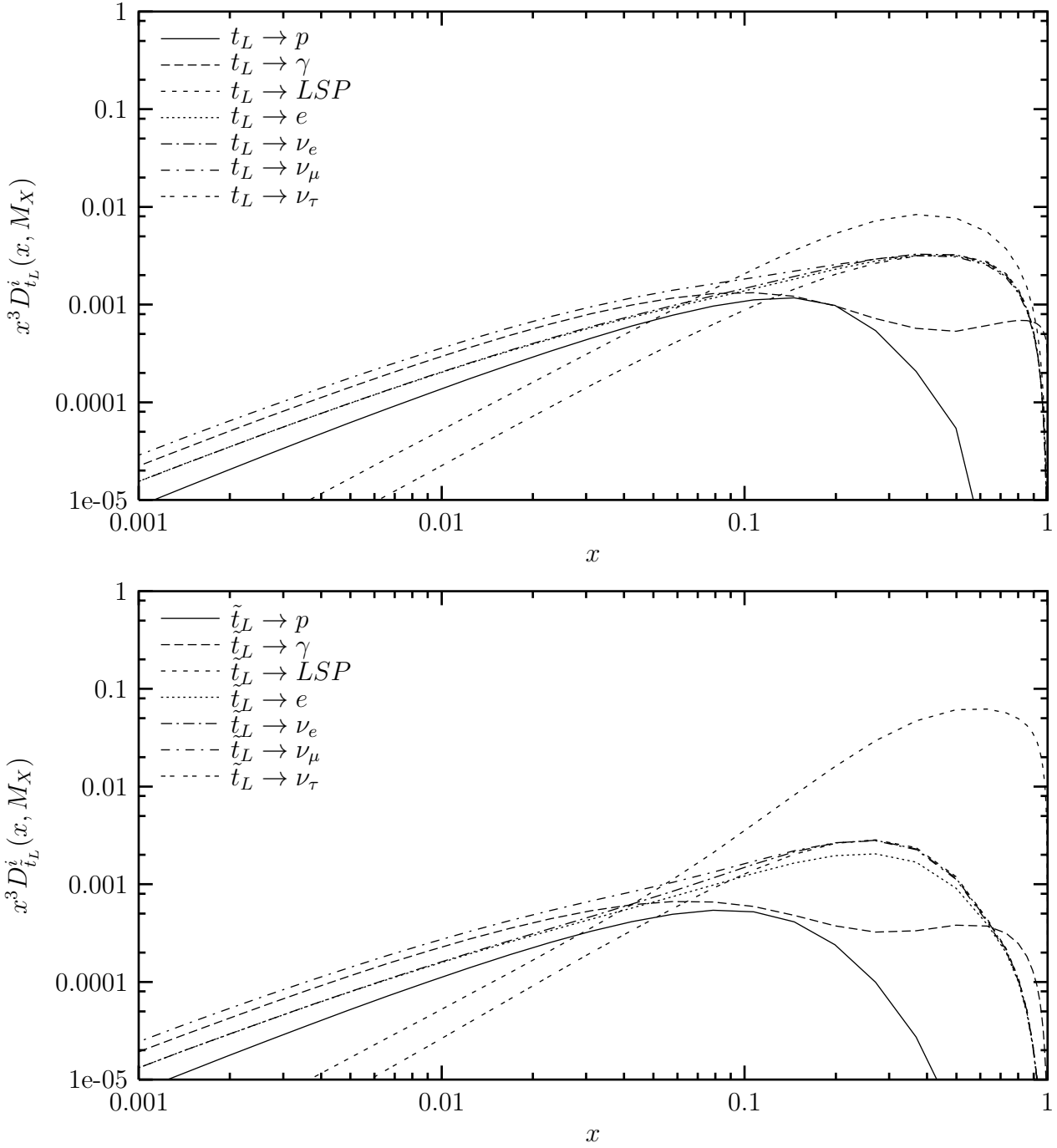


Figure 15: Fragmentation functions of a third generation $SU(2)$ doublet quark (top) and a squark (bottom) into stable particles.

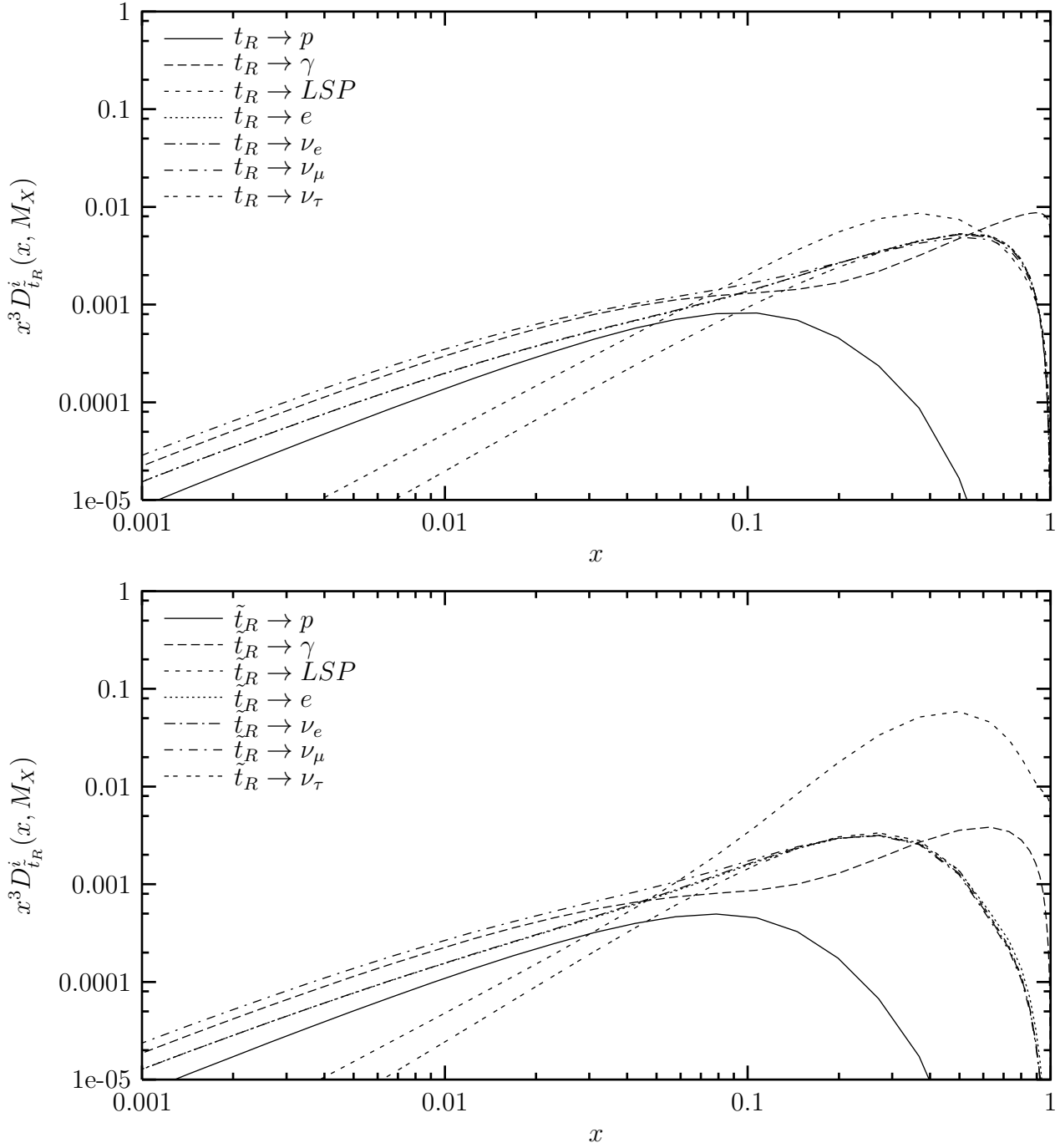


Figure 16: Fragmentation functions of a third generation $SU(2)$ singlet quark (top) and a squark (bottom) into stable particles.

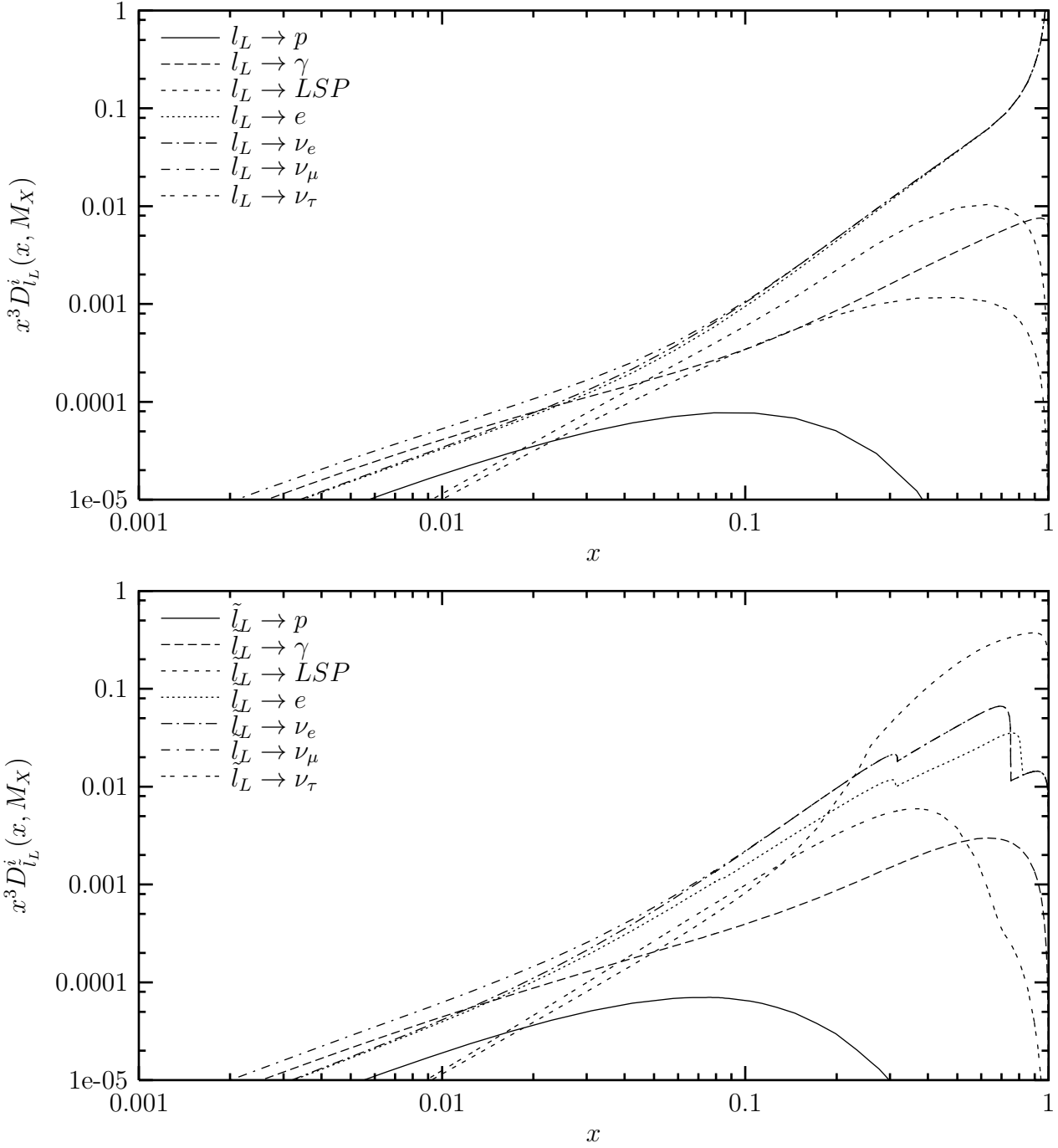


Figure 17: Fragmentation functions of a first or second generation $SU(2)$ doublet lepton (top) or slepton (bottom) into stable particles. The structures in some of the curves in the lower frame originate from 2-body decay kinematics.

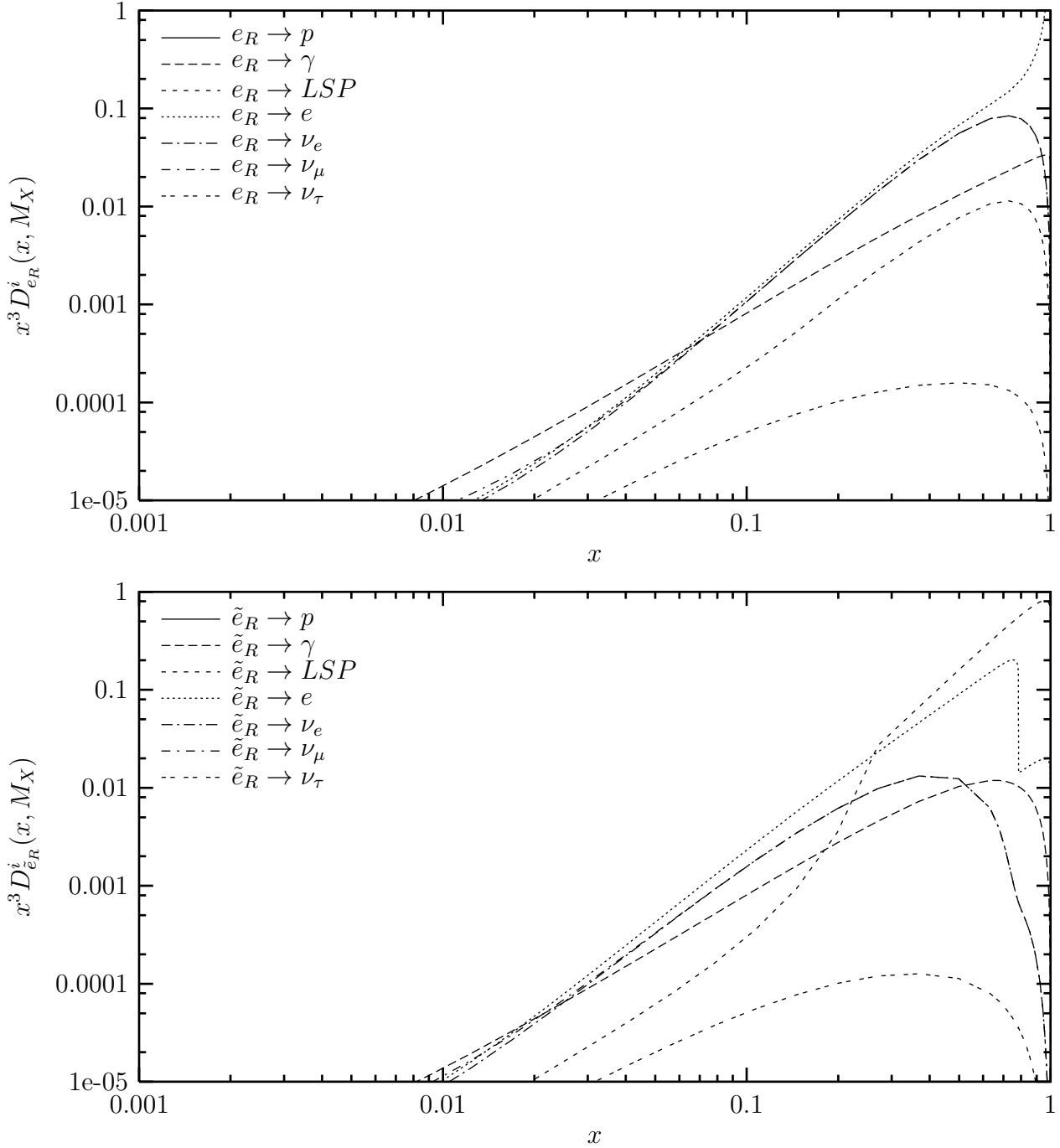


Figure 18: Fragmentation functions of a first or second generation $SU(2)$ singlet lepton (top) or slepton (bottom) into stable particles. The structures in some of the curves in the lower frame originate from 2-body decay kinematics.

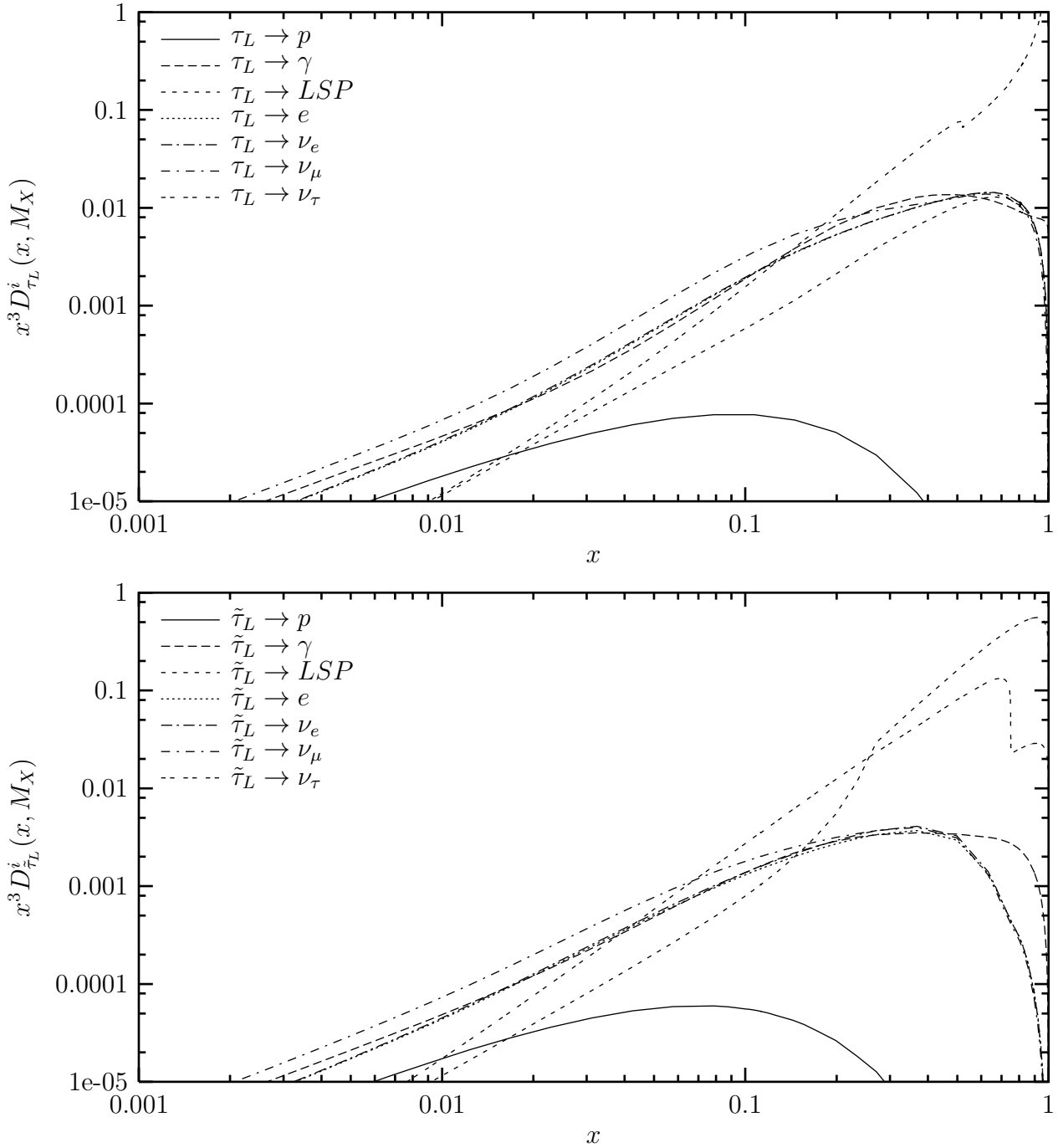


Figure 19: Fragmentation functions of a third generation $SU(2)$ doublet lepton (top) or slepton (bottom) into stable particles. The structures in some of the curves in the lower frame originate from 2-body decay kinematics.

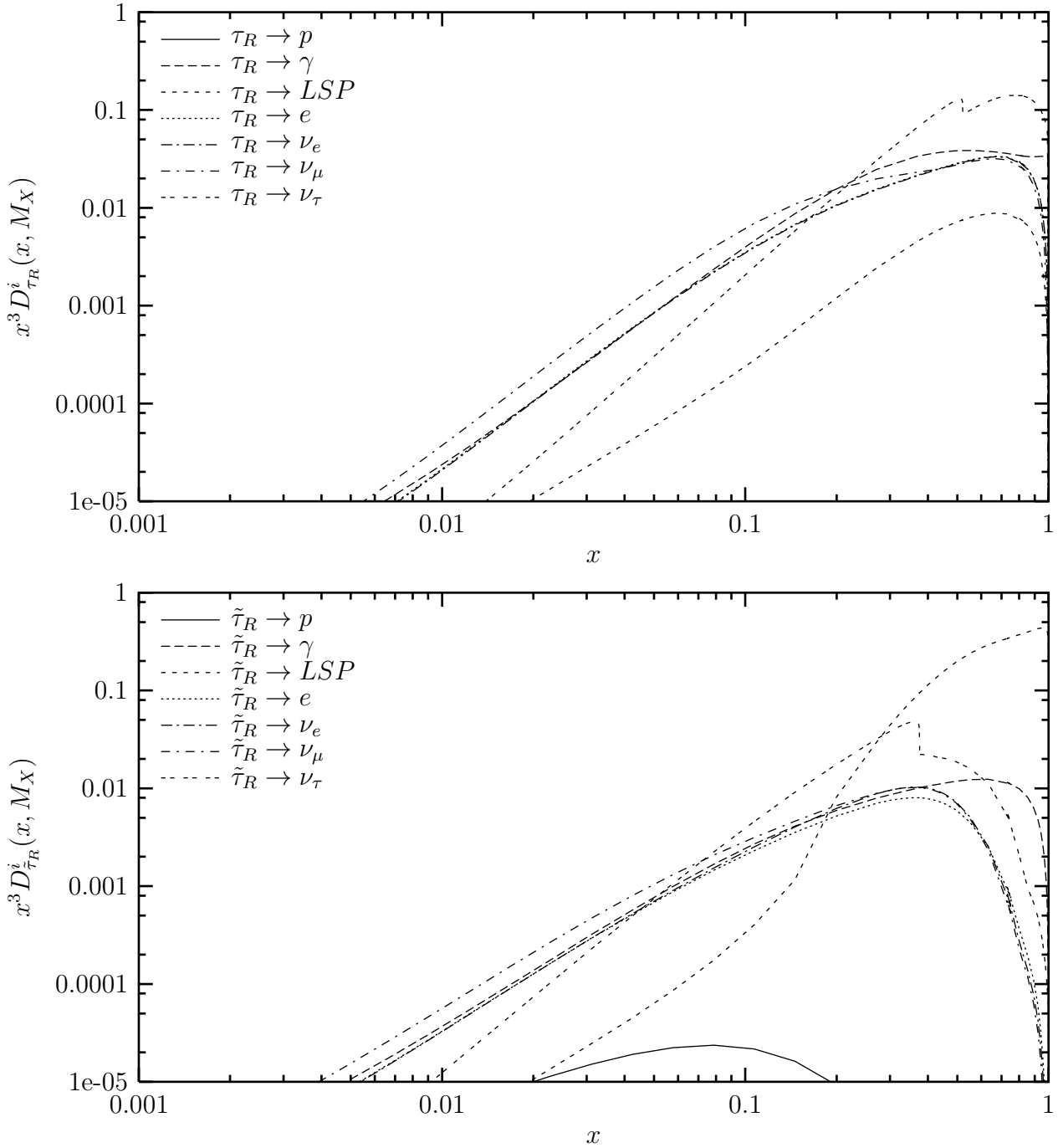


Figure 20: Fragmentation functions of a third generation $SU(2)$ singlet lepton (top) or slepton (bottom) into stable particles. The structures in some of the curves in the lower frame originate from 2-body decay kinematics.

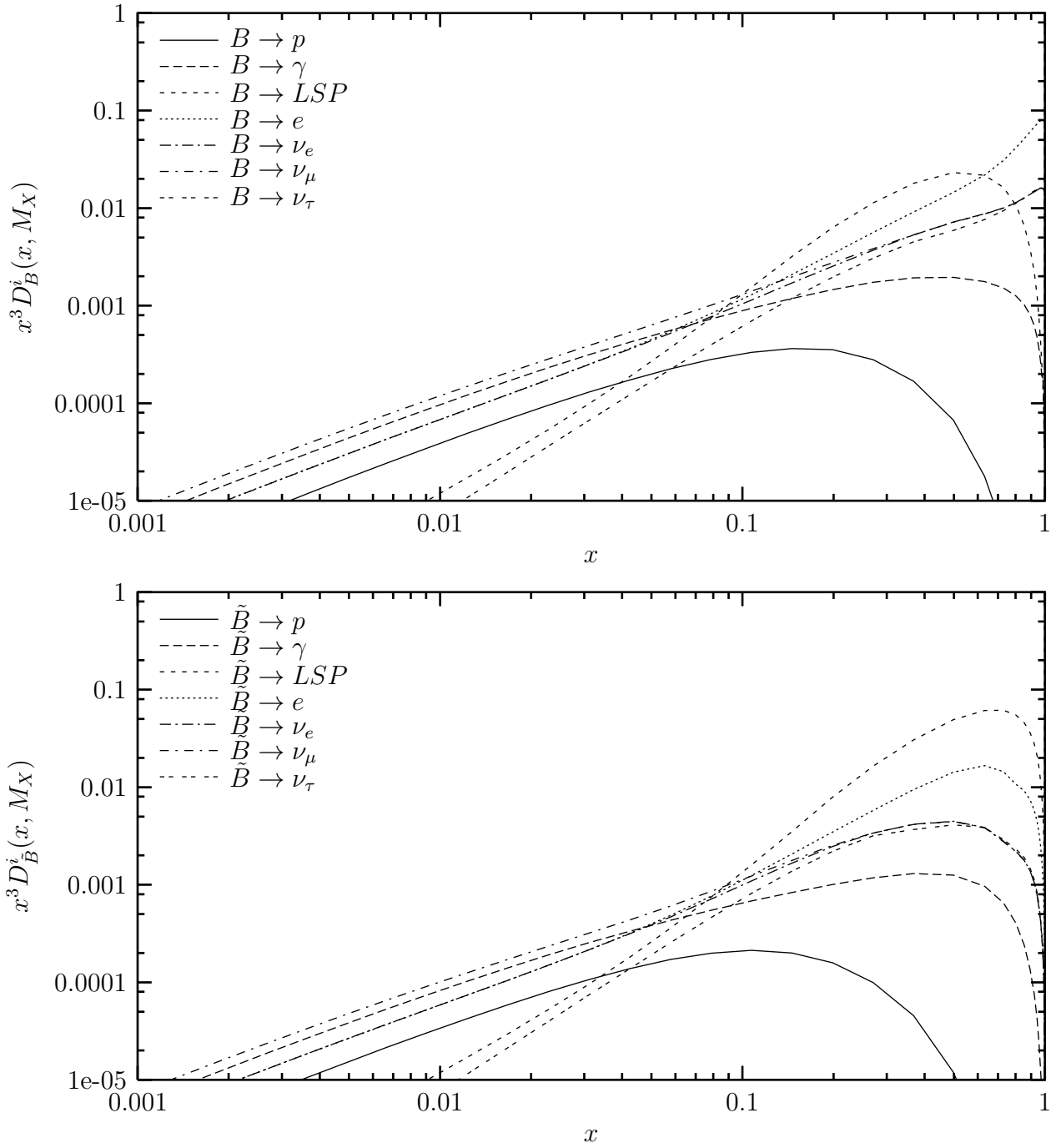


Figure 21: Fragmentation functions of a B boson(top) and a Bino (bottom) into stable particles.

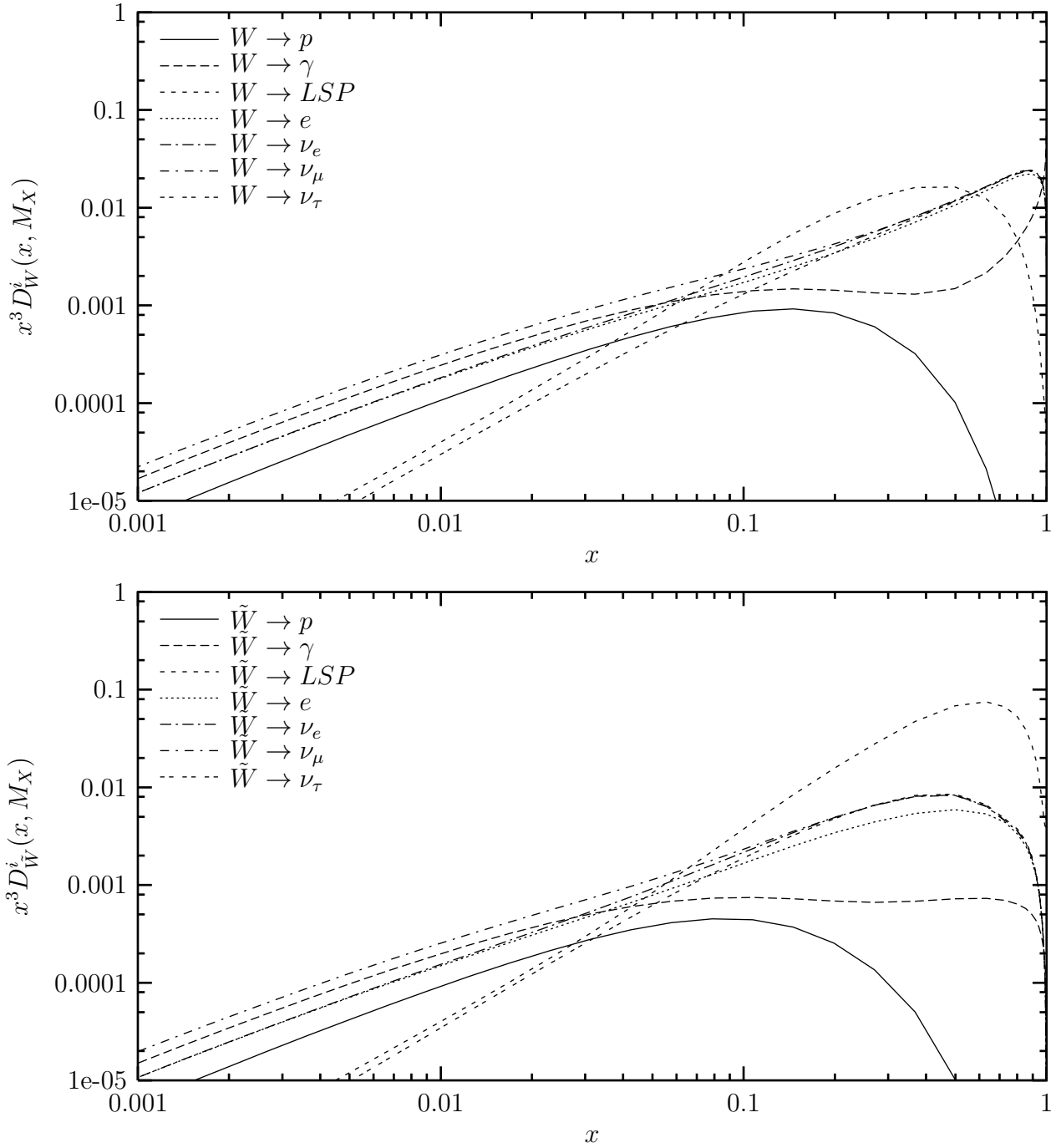


Figure 22: Fragmentation functions of a W boson (top) and a Wino (bottom) into stable particles.

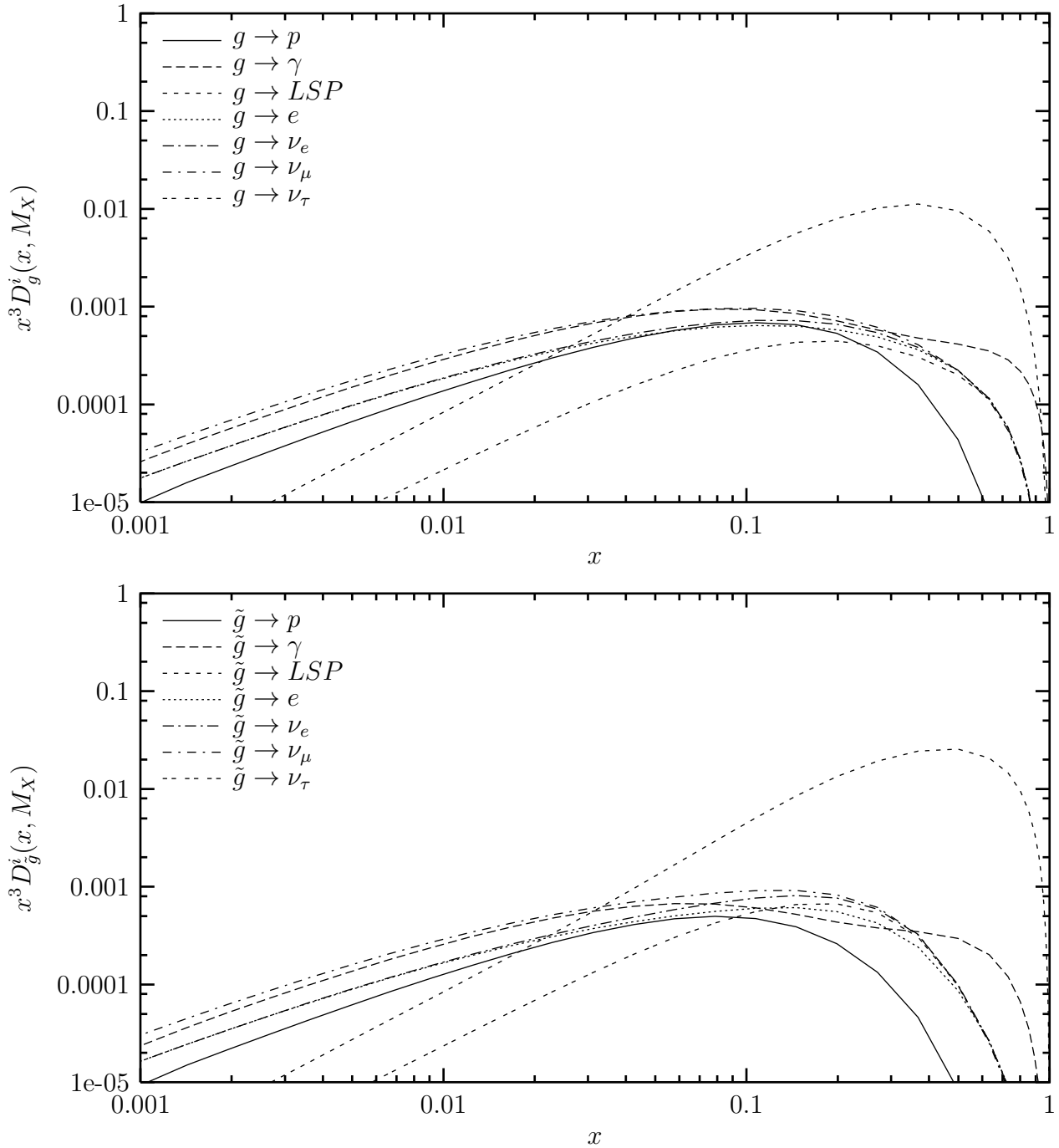


Figure 23: Fragmentation functions of a gluon (top) and a gluino (bottom) into stable particles.

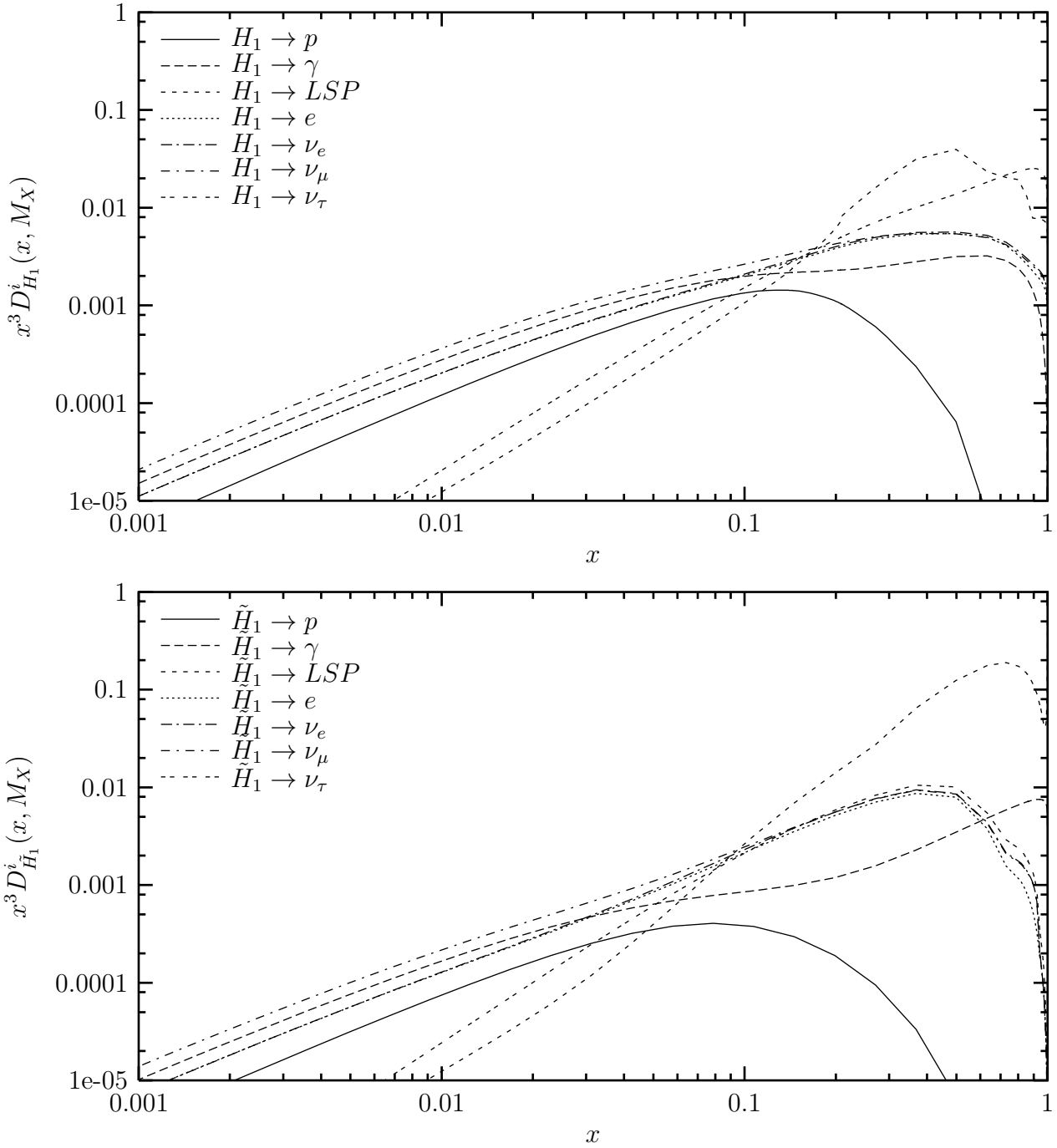


Figure 24: Fragmentation functions of a H_1 Higgs boson (top) and a \tilde{H}_1 higgsino (bottom) into stable particles.

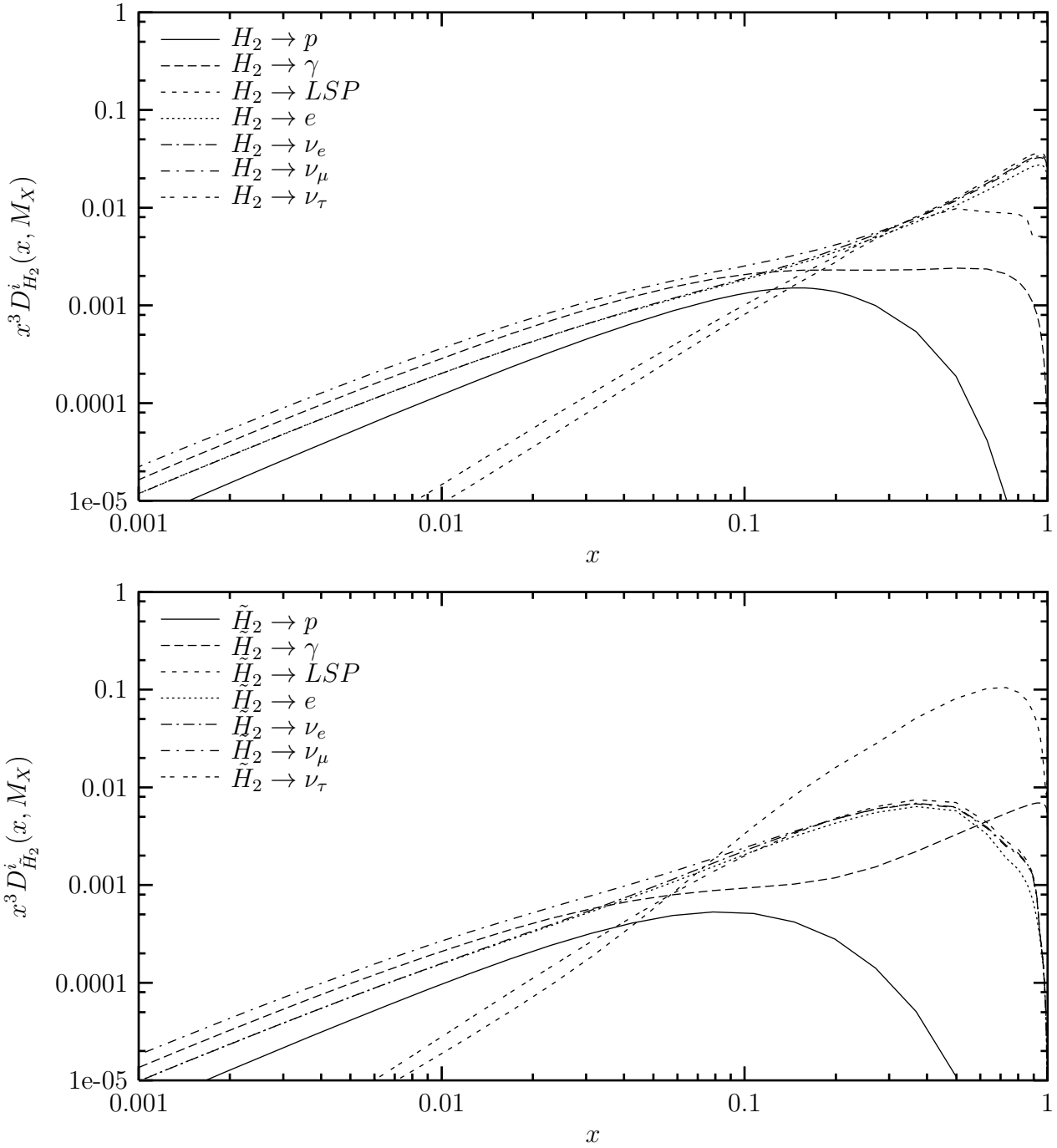


Figure 25: Fragmentation functions of a H_2 Higgs boson (top) and a \tilde{H}_2 higgsino (bottom) into stable particles.

References

- [1] K. Greisen, *Phys. Rev. Lett.* **16** (1966) 748; G. T. Zatsepin and V. A. Kuzmin, *JETP Lett.* **4** (1966) 78.
- [2] M. A. Lawrence, R. J. O. Reid, and A. A. Watson, *J. Phys.* **G17** (1991) 733; D. J. Bird *et al.*, *Astrophys. J.* **441** (1995) 144; HiRes-MIA collab., T. Abu-Zayyad *et al.*, *Astrophys. J.* **557** (2001) 686, astro-ph/0010652, and astro-ph/0208243; AGASA collab., N. Hayashida *et al.*, *Astrophys. J.* **522** (1999) 225, astro-ph/0008102; AGASA collab. M. Takeda *et al.*, astro-ph/0209422.
- [3] E. Waxman, *Phys. Rev. Lett.* **75** (1995) 386, astro-ph/9505082.
- [4] J. P. Rachen and P. L. Biermann, *Astron. Astrophys.* **272** (1993) 161, astro-ph/9301010.
- [5] E. Boldt and P. Ghosh, astro-ph/9902342.
- [6] P. Bhattacharjee and G. Sigl, *Phys. Rept.* **327** (2000) 109, astro-ph/9811011.
- [7] S. Sarkar, hep-ph/0202013.
- [8] C.T. Hill, D.N. Schramm and T.P. Walker, *Phys. Rev.* **D36**, (1987) 1007; P. Bhattacharjee, C.T. Hill and D.N. Schramm, *Phys. Rev. Lett.* **69** (1992) 567.
- [9] P. Bhattacharjee and G. Sigl, *Phys. Rev.* **D51** (1995) 4079, astro-ph/9412053; V. Berezhinsky and A. Vilenkin, *Phys. Rev. Lett.* **79** (1997) 5202, astro-ph/9704257.
- [10] J. Ellis, J. Lopez and D.V. Nanopoulos, *Phys. Lett.* **B247** (1990) 257; S. Chang, C. Coriano and A.E. Faraggi, *Nucl. Phys.* **B477** (1996) 65, hep-ph/9605325; K. Benakli, J.R. Ellis and D.V. Nanopoulos, *Phys. Rev.* **D59** (1999) 047301, hep-ph/9803333; K. Hamaguchi, Y. Nomura and T. Yanagida, *Phys. Rev.* **D58** (1998) 103503, hep-ph/9805346, and *Phys. Rev.* **D59** (1999) 063507, hep-ph/9809426; K. Hamaguchi, K.I. Izawa, Y. Nomura and T. Yanagida, *Phys. Rev.* **D60** (1999) 125009, hep-ph/9903207; C. Coriano, A.E. Faraggi and M. Plümacher, *Nucl. Phys.* **B614** (2001) 233, hep-ph/0107053.
- [11] D.J.H. Chung, E.W. Kolb and A. Riotto, *Phys. Rev.* **D60** (1999) 0603504, hep-ph/9809453; D.J. Chung, P. Crotty, E.W. Kolb and A. Riotto, *Phys. Rev.* **D64** (2001) 043503, hep-ph/0104100; R. Allahverdi and M. Drees, *Phys. Rev. Lett.* **89** (2002) 091302, hep-ph/0203118, and *Phys. Rev.* **D66** (2002) 063513, hep-ph/0205246.
- [12] V. Berezhinsky, M. Kachelriess, and A. Vilenkin, *Phys. Rev. Lett.* **79** (1997) 4302, astro-ph/9708217; V. A. Kuzmin and V. A. Rubakov, *Phys. Atom. Nucl.* **61** (1998) 1028, astro-ph/9709187; E.W. Kolb, D.J. Chung and A. Riotto, hep-ph/9810361, and *Phys. Rev.* **D59** (1999) 023501, hep-ph/9802238; H. Ziaepour, *Astropart. Phys.* **16** (2001) 101, astro-ph/0001137; V. Berezhinsky, *Nucl. Phys. Proc. Suppl.* **87** (2000) 387, hep-ph/0001163.

- [13] M. Birkel and S. Sarkar, *Astropart. Phys.* **9** (1998) 297, hep-ph/9804285.
- [14] K. Hagiwara and Y. Uehara, *Phys. Lett.* **B517** (2001) 383, hep-ph/0106320.
- [15] C. Barbot and M. Drees, *Phys. Lett.* **B533** (2002) 107, hep-ph/0202072.
- [16] V. Berezinsky and M. Kachelriess, *Phys. Rev.* **D63** (2001) 034007, hep-ph/0009053.
- [17] V.N. Gribov and L.N. Lipatov, *Yad. Fiz.* **15** (1972) 781, *Sov. J. Nucl. Phys.* **15** (1972) 438; G. Altarelli and G. Parisi, *Nucl. Phys.* **B126** (1977) 298; Y.L. Dokshitzer, *Sov. Phys. JETP* **46** (1977) 641, *Zh. Eksp. Teor. Fiz.* **73** (1977) 1216.
- [18] N. Rubin, PhD thesis, <http://www.stanford.edu/nrubin/Thesis.ps>.
- [19] C. Coriano and A. E. Faraggi, *Phys. Rev.* **D65** (2002) 075001, hep-ph/0106326.
- [20] S. Sarkar and R. Toldra, *Nucl. Phys.* **B621** (2002) 495, hep-ph/0108098.
- [21] Z. Fodor and S.D. Katz, *Phys. Rev. Lett.* **86** (2001) 3224, hep-ph/0008204.
- [22] A. Ibarra and R. Toldra, *JHEP* **0206**, (2002) 006 hep-ph/0202111.
- [23] V. Berezinsky, M. Kachelriess and S. Ostapchenko, *Phys. Rev. Lett.* **89** (2002) 171802, hep-ph/0205218.
- [24] H. Baer, F. E. Paige, S. D. Protopopescu, and X. Tata, hep-ph/9305342.
- [25] B. A. Kniehl, G. Kramer, and B. Pötter, *Nucl. Phys.* **B582** (2000) 514, hep-ph/0010289.
- [26] E. Reya, *Phys. Rept.* **69** (1981) 195.
- [27] S. K. Jones and C. H. Llewellyn Smith, *Nucl. Phys.* **B217** (1983) 145.
- [28] M. Ciafaloni, P. Ciafaloni and D. Comelli, *Phys. Rev. Lett.* **88** (2002) 102001, hep-ph/0111109.
- [29] V.S. Fadin, L.N. Lipatov, A.D. Martin and M. Melles, *Phys. Rev.* **D61** (2000) 094002, hep-ph/9910338; A. Denner, M. Melles and S. Pozzorini, hep-ph/0301241.
- [30] See e.g. K. Inoue, A. Kakuto, H. Komatsu and S. Takeshita, *Prog. Theor. Phys.* **71** (1984) 413.
- [31] U. Amaldi, W. de Boer and H. Fürstenau, *Phys. Lett.* **B260** (1991) 447; P. Langacker and M. Luo, *Phys. Rev.* **D44** (1991) 817; J. Ellis, S. Kelley and D.V. Nanopoulos, *Phys. Lett.* **B260** (1991) 131; C. Giunti, C.W. Kim and U.W. Lee, *Mod. Phys. Lett.* **A6** (1991) 1745.
- [32] Y.L. Dokshitzer, V.A. Khoze, A.H. Mueller and S.I. Troian, *Basics of Perturbative QCD*, Gif-sur-Yvette, France, Ed. Frontières (1991).

- [33] Y.I. Azimov, Y.L. Dokshitzer, V.A. Khoze and S.I. Troian, *Phys. Lett.* **B165** (1985) 147, and *Z. Phys.* **C27** (1985) 65.
- [34] W. Furmanski and R. Petronzio, *Z. Phys.* **C11** (1982) 293.
- [35] C. Peterson, D. Schlatter, I. Schmitt, and P. M. Zerwas, *Phys. Rev.* **D27** (1983) 105.
- [36] Recent analyses are: J.L. Feng, K.T. Matchev and F. Wilczek, *Phys. Lett.* **B482**, 388 (2000), [hep-ph/0004043](#); R. Arnowitt, B. Dutta and Y. Santoso, *Nucl. Phys.* **B606**,59 (2001), [hep-ph/0102181](#); J.R. Ellis et al., *Phys. Lett.* **B510**, 236 (2001), [hep-ph/0102098](#); A. Djouadi, M. Drees and J.-L. Kneur, *JHEP* **0108**, 055 (2001), [hep-ph/0107316](#); H. Baer et al., *JHEP* **0207**, 050 (2002), [hep-ph/0205325](#); A.B. Lahanas, D.V. Nanopoulos and V.C. Spanos, [hep-ph/0211286](#).
- [37] P. Gondolo, G. Gelmini and S. Sarkar, *Nucl. Phys.* **B392** (1993) 111, [hep-ph/9209236](#); F. Halzen and D. Hooper, *Rept. Prog. Phys.* **65** (2002) 1025, [astro-ph/0204527](#).
- [38] C. Barbot, M. Drees, F. Halzen and D. Hooper, [hep-ph/0205230](#).
- [39] C.P. Fong and B.R. Webber, *Phys. Lett.* **B229** (1989) 289.
- [40] V. Berezhinsky and M. Kachelriess, *Phys. Lett.* **B434** (1998) 61, [hep-ph/9803500](#).
- [41] R.A. Vazquez et al., *Astropart. Phys.* **3** (1995) 151; M. Ave et al., *Phys. Rev. Lett.* **85** (2000) 2244 (2000), [astro-ph/0007386](#), and *Phys. Rev.* **D65** (2002) 063007, [astro-ph/0110613](#); AGASA collab., K. Shinozaki et al., *Astrophys. J.* **571** (2002) L120.
- [42] C. Barbot, M. Drees, F. Halzen and D. Hooper, [hep-ph/0207133](#).
- [43] See e.g. S. P. Martin, [hep-ph/9709356](#).